Probabilistic Environmental Modeling System for Munitions Mobility
SERDP Project Number MR-2733

Margaret L. Palmsten[1]
Allison M. Penko[2]

[1]U.S. Geological Survey
[2]U.S. Naval Research Laboratory

September 2020

REPORT DOCUMENTATION PAGE

Form Approved
OMB No. 0704-0188

1. REPORT DATE *(DD-MM-YYYY)*	**2. REPORT TYPE**	**3. DATES COVERED** *(From - To)*
01-09-2020	SERDP Interim Report	1/23/2017 – 8/13/21

4. TITLE AND SUBTITLE

Probabilistic Environmental Modeling System for Munitions Mobility

5a. CONTRACT NUMBER

5b. GRANT NUMBER

5c. PROGRAM ELEMENT NUMBER

6. AUTHOR(S)

Margaret Palmsten
Allison Penko

5d. PROJECT NUMBER
MR-2733

5e. TASK NUMBER

5f. WORK UNIT NUMBER

7. PERFORMING ORGANIZATION NAME(S) AND ADDRESS(ES)

U.S. Geological Survey
Reston, VA 20192
USA

U.S. Naval Research Laboratory
Washington DC, 20375
USA

8. PERFORMING ORGANIZATION REPORT NUMBER

MR-2733

9. SPONSORING / MONITORING AGENCY NAME(S) AND ADDRESS(ES)

Strategic Environmental Research and Development Program
4800 Mark Center Drive, Suite 16F16
Alexandria, VA 22350-3605

10. SPONSOR/MONITOR'S ACRONYM(S)
SERDP

11. SPONSOR/MONITOR'S REPORT NUMBER(S)
MR-2733

12. DISTRIBUTION / AVAILABILITY STATEMENT

Distribution A: Approved for public release; distribution is unlimited.

13. SUPPLEMENTARY NOTES

14. ABSTRACT

The Strategic Environmental Research and Development Program's Underwater Munitions Response effort seeks to assess the environment where munitions are found over real-time and historical periods. A key aspect of understanding munitions mobility and burial in the underwater environment is being able to characterize the waves, currents, and morphologic change as a function of time. This document describes efforts to develop a modeling system to nowcast and hindcast the underwater environment where munitions are found. In the first year of the project, we focused on testing the capability of a coupled hydro- and morphodynamic model, Delft3D, to provide accurate hydrodynamics and morphodynamics. In the second and third year of the project, which is the focus of this report, we coupled Delft3D to the Underwater Munitions Expert System (UnMES). UnMES is a probabilistic model designed to estimate the mobility and burial of munitions. A primary result of this phase of the project was production of cartographic visualizations of UnMES results.

15. SUBJECT TERMS

Underwater Munitions Expert System, UnMES, munitions mobility, modeling

16. SECURITY CLASSIFICATION OF:			**17. LIMITATION OF ABSTRACT**	**18. NUMBER OF PAGES**	**19a. NAME OF RESPONSIBLE PERSON**
a. REPORT	**b. ABSTRACT**	**c. THIS PAGE**			Allison Penko
UNCLASS	UNCLASS	UNCLASS	UNCLASS	70	**19b. TELEPHONE NUMBER** *(include area code)* 228-688-4823

Table of Contents

List of Tables

List of Figures

List of Acronyms

BSS	-	Brier Skill Score
C	-	Chézy coefficient
CDIP	-	Coastal Data Information Program
COR	-	Correlation coefficient
CRAB	-	Coastal Research Amphibious Buggy
CRMSD	-	Centered root-mean-square difference
DSRC	-	Department of Defense Supercomputing Resource Center
DEM	-	Digital Elevation Model
FLOW	-	Flow module in Delft3D
FRF	-	Field Research Facility
GLUE	-	Generalized Likelihood Uncertainty Estimation
h	-	water depth
H_s	-	Significant wave height
LARC	-	Lighter Amphibious Resupply Cargo
MOR	-	Morphology module in Delft3D
MR	-	Munitions Response
MRSON	-	Munitions Response Statement of Need
n	-	Manning's friction coefficient
N	-	Number of data points in time series χ
NAVFAC	-	Naval Facilities Engineering Command
NOAA	-	National Oceanic and Atmospheric Administration
RMS	-	Root-mean-square
RMSD	-	Root-mean-square difference
RMAE	-	Relative mean absolute error
SERDP	-	Strategic Engineering Research and Development Program
STD	-	Standard deviation
SWAN	-	Simulating WAves Nearshore, 3rd generation wave model
θ	-	Wave direction at peak period
T_p	-	Peak wave period
UnMES	-	Underwater Munitions Expert System
u	-	Cross-shore component of velocity
UXO	-	Unexploded ordnance
v	-	Alongshore component of velocity
WAVE	-	Wave module in Delft3D, i.e., SWAN
x	-	Cross-shore axis of local coordinate system
χ_m	-	Hydrodynamic or morphodynamic simulation output parameter
χ_o	-	Hydrodynamic or morphodynamic observation
y	-	Alongshore axis of local coordinate system
z_i	-	initial bed level at beginning of simulation
z_m	-	Simulated bed level
z_o	-	Observed bed level

Acknowledgements

We would like to thank the staff of the U.S. Army Corps of Engineers Field Research Facility for data collection and archiving. Without their excellent work, this research would not be possible. We also thank Jay Veeramony for offering advice on Delft3D model setup.

Abstract

The Strategic Environmental Research and Development Program's (SERDP) Underwater Munitions Response effort seeks to assess the environment where munitions are found over real-time and historical periods. A key aspect of understanding munitions mobility and burial in the underwater environment is being able to characterize the waves, currents, and morphologic change as a function of time. This document describes efforts to develop a modeling system to nowcast and hindcast the underwater environment where munitions are found. In the first year of the project, we focused on testing the capability of a coupled hydro- and morphodynamic model, Delft3D, to provide accurate hydrodynamics and morphodynamics. In the second and third year of the project, which is the focus of this report, we coupled Delft3D to the Underwater Munitions Expert System (UnMES). UnMES is a probabilistic model designed to estimate the mobility and burial of munitions. A primary result of this phase of the project was production of cartographic visualizations of UnMES results. Additionally, we further tested Delft3D and compared results of the coupled Delft3D/UnMES system with observations of surrogate munitions. The overall scientific objective of the project is to determine whether estimates of hydrodynamics and morphologic change improve hindcasts of munitions mobility and burial. The payoff is the capability to produce maps of munitions mobility and burial for site managers.

1. Objectives

1.1. Project objective

MR-2733 was designed in response to the fiscal year 2017 Statement of Need for the Munitions Response Program Area (MRSON-17-01), which seeks to assess the environment in which munitions are found over real-time and historical periods. The overall objective of MR-2733 is to develop ensemble hindcasts of waves, currents, and sediment transport, including uncertainties, using a state-of-the-art hydrodynamic and morphologic change model at underwater munitions remediation sites. Simulations will be coupled to an existing probabilistic model, Unexploded Munitions Expert System (UnMES, MR-2645), which presently lacks the necessary time-dependent forcing conditions to provide reliable estimates of munitions mobility and burial. The coupled modeling system will ultimately be used to develop cartographic visualizations of the probability of munitions mobility and burial over both long-term/historic and short-term timescales. The products from this effort will provide managers at munitions response sites with the best available tools for cost-effective decision-making. As such, our simulation results will merge seamlessly with risk assessment and management tools. Important scientific questions relate to the roles of time-dependence and uncertainty in modeling munitions mobility. Our work will address the following questions:

1) How do improved estimates of hydrodynamics and morphologic change improve historical estimates of munitions mobility and burial?
2) What is the role of time-dependence in estimating the probability of munitions mobility and burial?
3) What is the effect of hydrodynamic and morphologic uncertainty on our understanding of the probability of munitions mobility and burial?

1.2. Background

Previous SERDP findings have identified morphologic change as an important mechanism for munitions mobility. For example, MR-2320 identified sand wave migration off the coast of Panama City, FL as the cause of object burial during storms over the April-May 2013 deployment of instrumentation and surrogate munitions. Likewise, MR-2319 found that mega-ripples and sand waves with wavelengths of (O) 100 m and heights of 3 m caused surrogate munitions exposure and burial in tidally dominated areas between Martha's Vineyard and Nantucket, MA. Observations and modeling at Camp Perry, OH on Lake Erie, in "Vortex Lattice Unexploded Ordnance (UXO) Mobility Integration" (MR-201234), identified shoreline erosion as a primary cause of munitions exposure, even after extensive surveys and beach clearance efforts had resulted in the area being declared free of munitions. Additionally, the Naval Facilities Engineering Command (NAVFAC) report, "Hydrodynamic Analysis of UXO Transport Andrew Bay" identified storm related erosion and deposition or "beach churn", as one of the primary drivers of munitions exposure on the cobble beach at the former Adak Naval Complex in Adak, AK.

Our work leverages several existing Strategic Environmental Research and Development Program (SERDP) funded efforts. SERDP projects have recently focused on near-field models that predict the munitions response for given far-field hydrodynamic and morphologic conditions. Presently, near-field model forcing relies on historical (long-time-series) observations of waves and a simple wave transformation model. Near-field munitions mobility and burial models presently allow only a rudimentary estimate of morphologic change based on observations, which are unavailable at most remediation sites. Near-field models also neglect time-dependence, which is likely important for understanding munitions mobility for timescales of less than a year. Our effort provides state-of-the-art probabilistic and time-dependent far-field forcing conditions to drive the existing near-field models for munitions exposure/burial and migration. The near-field efforts can be divided into deterministic and

probabilistic approaches. The SERDP projects titled "Simple Parameterized Model for Predicting Mobility, Burial and Re-Exposure of Underwater Munitions" (MR-2224) and "Parameterized Process Models for Underwater Munitions Expert System" (MR-2647) employ deterministic approaches. Both projects estimate scour-burial of munitions by identifying relationships between environmental conditions and munitions properties. The SERDP projects titled "Underwater Munitions Expert System to Predict Mobility and Burial" (MR-2227) and "Underwater Munitions Expert System for Remediation Guidance" (MR-2645) employ probabilistic approaches. MR-2227 and MR-2645 build on the deterministic approach by developing probabilistic models from many realizations of the deterministic models under a wide range of forcing conditions. Both probabilistic projects aim to predict the likelihood of migration and burial. Far-field forcing conditions from a hydro- and morphodynamic model are necessary inputs to drive near-field models.

Our overall technical approach for the project includes three primary steps to provide probabilistic visualizations of munitions mobility and burial to the end user (Figure 1). In Year 1 of the project we created a suite of environmental initial and boundary conditions based on historical point observations at our initial study site on the Outer Banks of North Carolina (Figure 1a). We ran ensembles of hydrodynamic and morphologic simulations and adapted an existing methodology to produce a probabilistic representation of spatially and temporally varying conditions (Figure 1b). In the second and third year, in collaboration with Dr. Sarah Rennie and Dr. Alan Brandt (MR-2645), we integrated the probabilistic spatially and temporally varying far-field conditions (e.g., water depth, wave direction, bottom velocity, sediment erosion/accretion) into the near-field probabilistic model, UnMES (Figure 1c), which resulted in estimates of the probability of munitions mobility for a particular location and time. Additionally, we created prototype cartographic visualizations of the probability of munitions mobility and environmental conditions across the site area based on the coupled near- and far-field models (Figure 1d) for time-dependent (storm time-scale) forcing. These visualizations are the prototype for eventual transition to operational use.

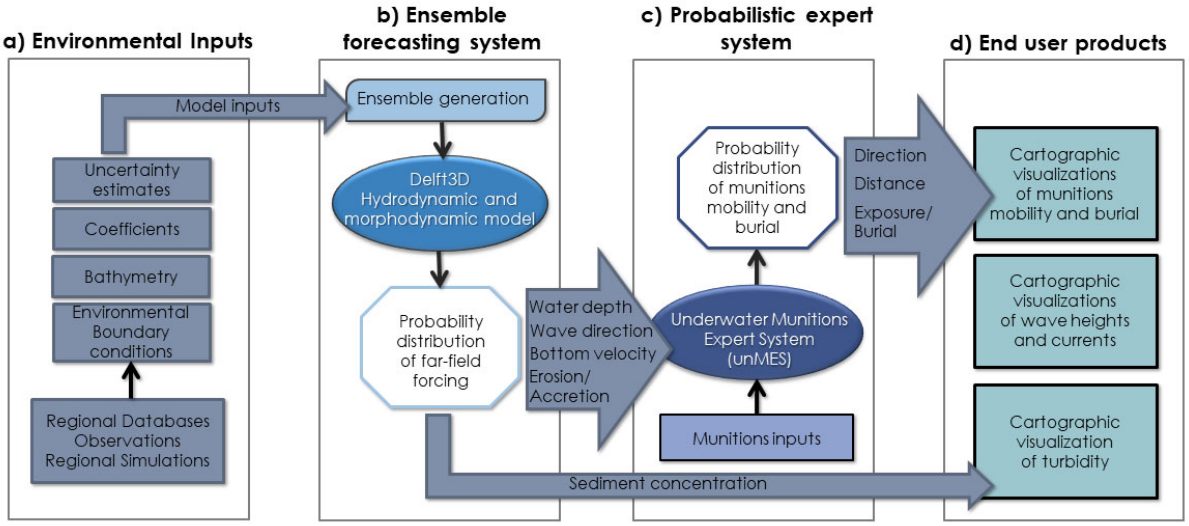

Figure 1. Flow chart describing the probabilistic environmental forecasting system for munitions mobility and burial. Panel a) leverages an existing U.S. Naval Research Laboratory base funded project that will provide initial and boundary conditions to the far-field model when in situ or historical data inputs are unavailable. Panel b) was the focus of the first year of the project. Panels c) and d) were the focus of Years 2 and 3, with coupling of UnMES in cooperation with Dr. Rennie and Dr. Brandt. Panel d) describes the prototype visualizations for eventual transition to operations.

1.3. Report objectives

The objective of this report is to document the progress in the second and third year toward the overall objective of the project, which is focused on incorporating results from the hydrodynamic and morphodynamic model, Delft3D, to UnMES (Figure 1). To accomplish our objective, we developed the one-way coupled Delft3D-UnMES system and compared hydrodynamic and morphodynamic simulations to observations of wave height, wave frequency, wave direction, depth-averaged current velocity, and sediment erosion and accretion. We then compared estimates of the probability of munitions mobility and burial to observations of surrogate munitions behavior during a field experiment in Jan/Feb 2015 at the U.S. Army Corps of Engineers Field Research Facility (FRF) in Duck, NC. In this report we present a quantitative analysis of model results for three time periods. The environmental conditions that occurred during the time periods include a Northeaster storm in January 2015, Hurricane Joaquin in October 2015, the exposure of historic practice munitions on the beach, and Hurricane Dorian in September 2019.

2. Technical approach

2.1. Study site and simulated conditions

The primary study site for MR-2733 is the U.S. Army Corps of Engineers Field Research Facility (FRF) (http://www.frf.usace.army.mil/frf.shtml), located on a sandy Atlantic coast beach in Duck, NC, USA (Figure 2a). The Navy and Air Force used the site as a bombing and rocket-fire range between 1945 and 1969, and since the establishment of the FRF in 1977, it is recognized as a world-premiere coastline observatory. We chose the study site to leverage ongoing projects at FRF, including projects funded by SERDP (e.g., MR-2320), U.S. Army Corps of Engineers, U.S. Geological Survey, and Office of Naval Research, to test the modeling system. Rennie and Brandt (2015) developed the prototype version of UnMES (MR-2227) with data from the FRF. Existing in situ infrastructure at the FRF supports the long-time-series measurements of waves, currents, and bathymetric surveys used in this study.

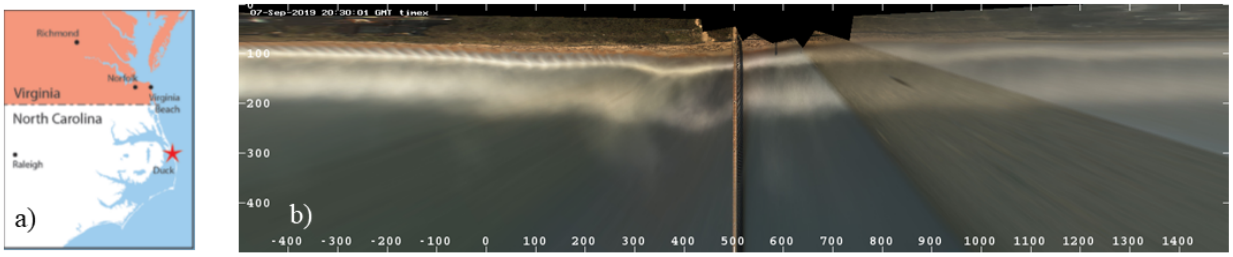

Figure 2. a) Location of the U.S. Army Corps Field Research Facility (FRF) and b) time exposure Argus image from 7 September 2015 at 2030 GMT (1530 EDT) in the local FRF-coordinate system after the passage of Hurricane Dorian. Wave breaking over the sandbar is represented by white pixels in the time exposure image. The FRF pier is located at y = 500 m.

The geomorphology of the study site is typical of a barrier island on the east coast of the United States and helps define the local coordinate system. The beach is backed by an extensive dune system and one or more sandbars are typically present (e.g., Figure 2b). The shoreline at the FRF is oriented ~18° north-northwest of true north, and the local coordinate system is defined relative to the shoreline, with the x-axis oriented in the cross-shore direction and the y-axis oriented in the alongshore direction Figure 2b). The climatological intertidal beach slope is 0.08 (Plant and Holman, 1997), and beach slope flattens

offshore. Grain size ranges between coarse and fine sand with median grain size decreasing across the nearshore region (Stauble, 1992).

In this report, we simulated three storm periods (Table 1). One simulation consisted of a series of Northeaster storms with intermittent calm periods that passed between 26 January and 15 February 2015 during the SERDP munitions mobility experiment under MR-2320 (Figure 3 and Figure 4). As previously reported, we simulated wave conditions between 2 and 8 October 2015. A Northeaster storm passed during this period, followed by the passage of Hurricane Joaquin offshore of the FRF (Figure 5 and Figure 6). The third simulation period was between 2 and 8 September when Hurricane Dorian made landfall at Cape Hatteras, NC as a Category 2 storm on the Saffir-Simpson Scale (Figure 7 and Figure 8). Maximum significant wave heights during the three periods modeled exceeded the 99th percentile for the FRF wave climatology.

Table 1. Wave conditions at the Waverider buoy located in 26 m water depth for the simulation periods included in these analyses Surge observations come from the FRF NOAA tide station on the pier.

Simulation period	**Storm**	**Significant wave height, H_s (m)**	**Peak wave period, T_p (s)**	**Median wave direction, θ (Degrees)**	**Maximum surge (m)**
26 Jan – 15 Feb	Northeaster	0.5 – 5.0	3 – 15	75	0.72
2-8 Oct 2015	Northeaster/Joaquin	1.0 – 5.0	7 – 13	90	0.97
2-8 Sep 2019	Dorian	0.7 – 6.8	4 – 13	115	1.11

Figure 3. Conditions at the peak of a Northeaster storm on 11 February 2015 at 0830 EST during munitions mobility and burial experiment were simulated using Delft3D. The surf zone extended offshore of the end of the FRF pier.

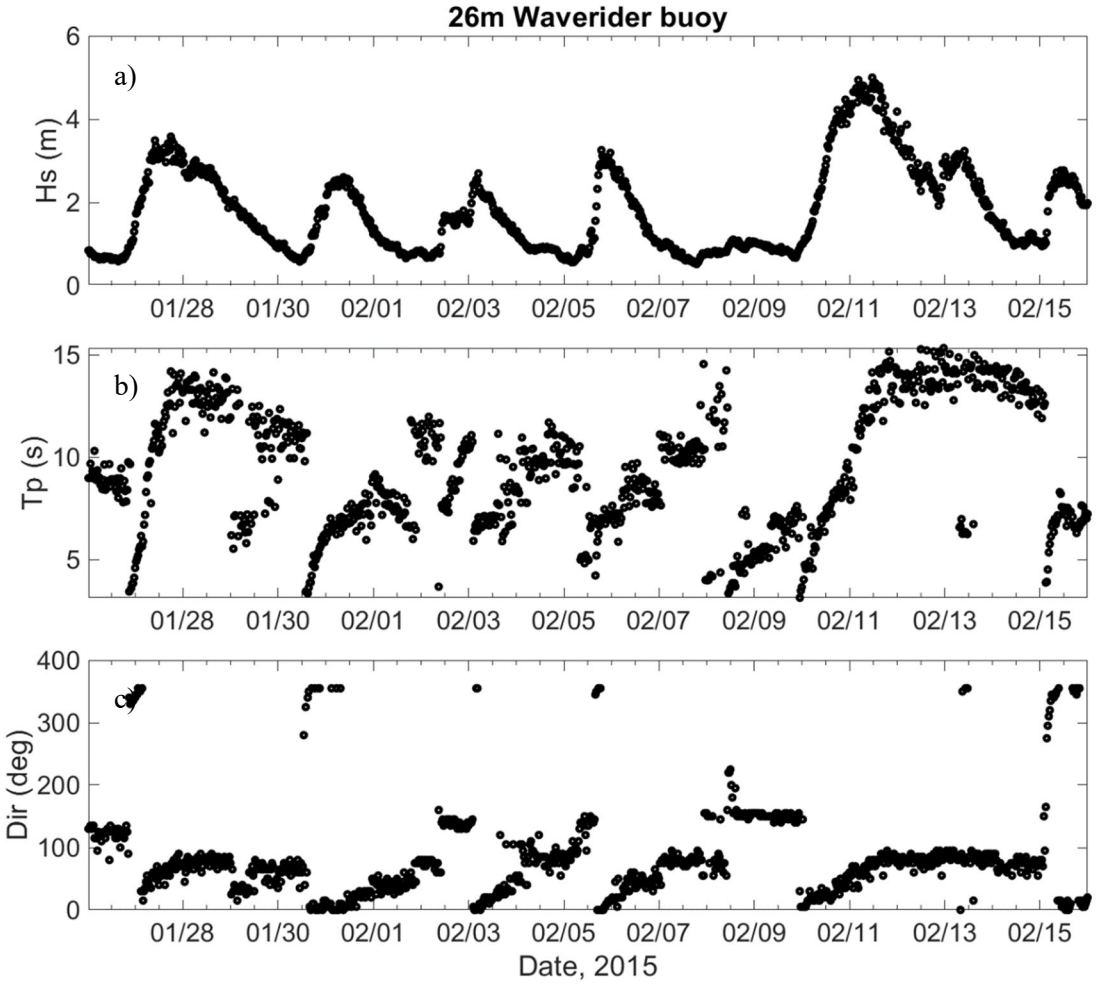

Figure 4. Offshore (a) significant wave height, H_s, (b) peak wave period, T_p, and (c) wave direction at peak period, Dir, from buoy at CDIP Station 430 in 26-m water depth for the munitions mobility experiment simulated in this report. A series of Northeaster storms occurred during the simulation period.

Figure 5. Conditions in the surf zone as Hurricane Joaquin passed offshore on 5 October 2015.

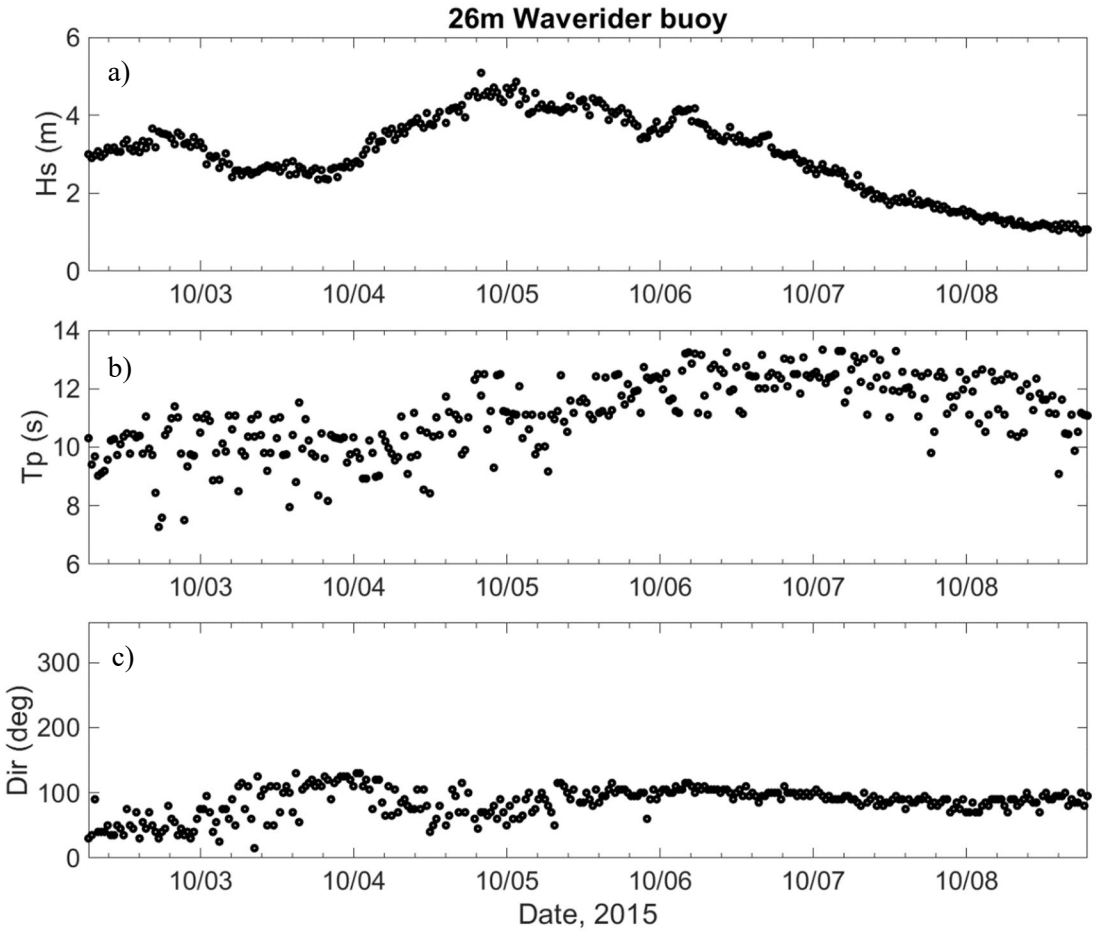

Figure 6. Offshore (a) significant wave height, H_s, (b) peak wave period, T_p, and (c) wave direction at peak period, Dir, from buoy at CDIP Station 430 in 26-m water depth. A Northeaster storm (first peak in wave height) and Hurricane Joaquin (second peak in wave height) occurred during the simulation period.

Figure 7. Conditions at 1600 EDT on 6 September 2019 during the passage of Hurricane Dorian. Imagery courtesy of the Coastal Imaging Lab at Oregon State University.

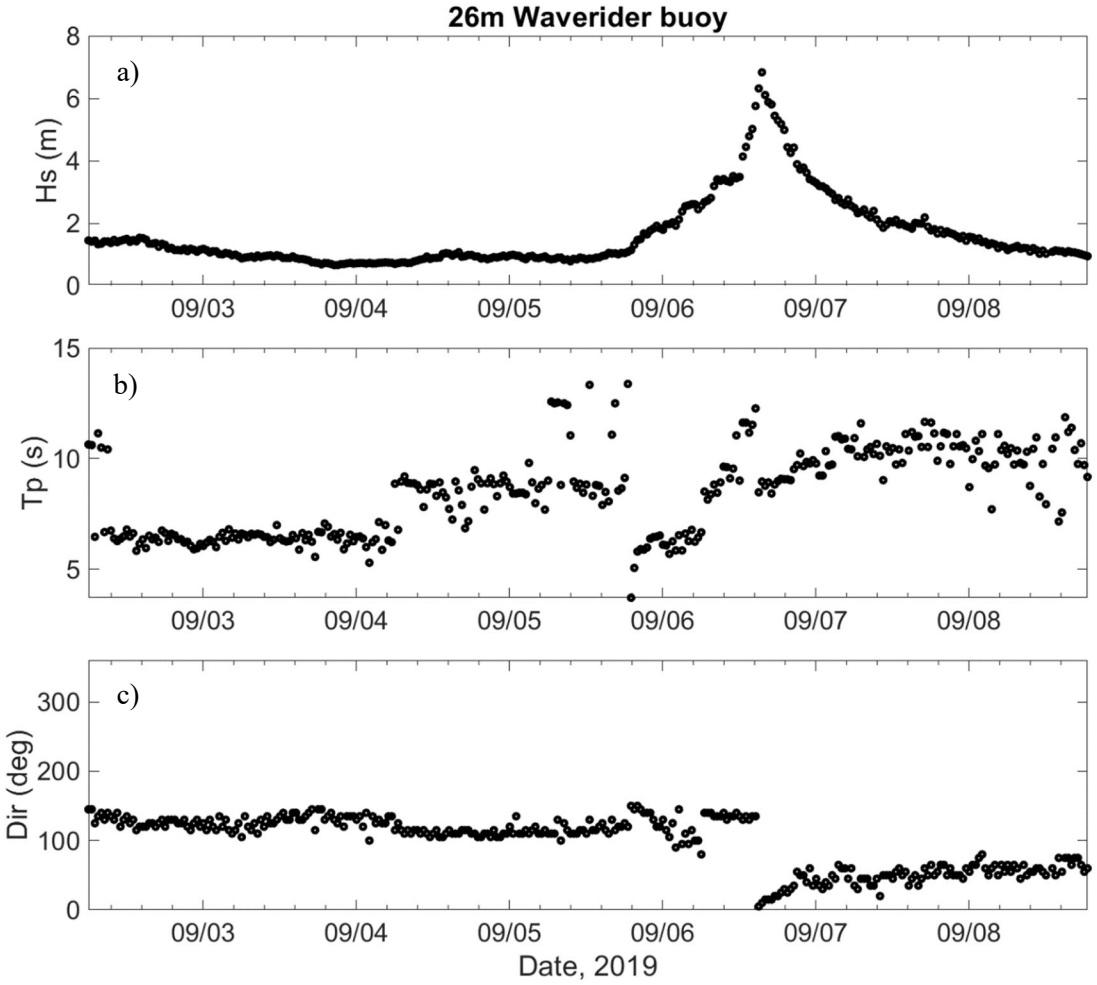

Figure 8. Offshore (a) significant wave height, H_s, (b) peak wave period, T_p, and (c) wave direction at peak period, Dir, from buoy at CDIP Station 430 in 26-m water depth during the period when Hurricane Dorian made landfall at Cape Hatteras, NC.

2.2. Wave, current, seafloor elevation, and munitions mobility observations

Simulated waves and currents were compared to observations collected by instruments that are part of the long-term FRF data array located within the inner grid model domain (model domain is described in Section 2.5) (Figure 9). Significant wave height, peak wave period, and wave direction at peak period were compared to observations from a pressure array in 8-m water depth (36° 11.23' N, 75° 44.57' W) (Figure 9). Depth-averaged current speed and direction were compared to observations from a current

profiler located in 6-m of water (36° 11.24' N, 75° 44.79' W) and 11-m of water (36° 11.36' N, 75° 44.36' W).

During the munitions mobility experiment in January-March 2015, an additional mooring was deployed in 8-m water depth, measuring waves, currents, and the mobility and burial of surrogate munitions (Figure 9, yellow circle). The suite of munitions was composed of three 155-mm Howitzer surrogates, two 81-mm mortar surrogates and two small caliber bullet surrogates. The surrogate munitions had a range of densities approximately equal to or denser than quartz sand. All surrogates were observed to bury in in place (Figure 10).

Figure 9. Location of instrumentation used for comparison with simulations plotted on Google Earth imagery.

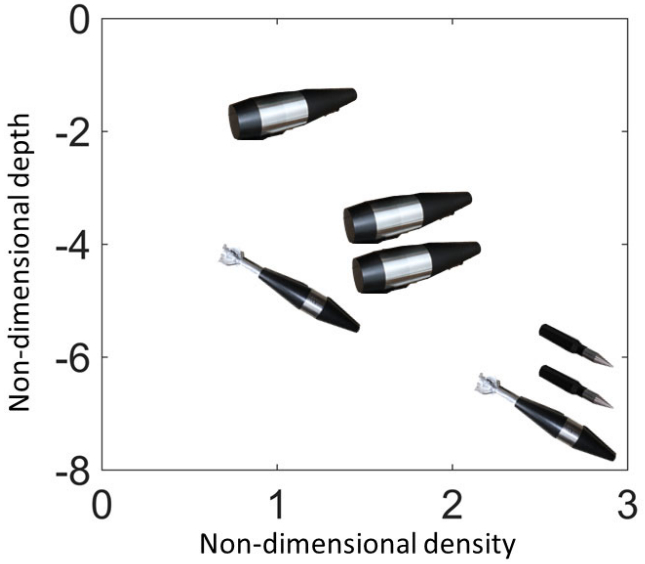

Figure 10. Non-dimensional burial depth (ratio of munitions burial depth to munitions diameter) plotted with non-dimensional density (ratio of munitions density to sand density) of surrogate munitions during January-March 2015 experiment conducted as part of MR-2320.

2.3. Bathymetric observations

Bathymetry is required to provide an initial bottom boundary condition to the model, as well as to evaluate simulations of morphologic change. Bathymetry was defined using digital elevation model (DEM) developed for numerical modeling at the FRF (Young et al., 2018) and hydrographic surveys conducted prior to and after each simulation period. Surveys were conducted with one of two vehicles. The Lighter Amphibious Resupply Cargo (LARC) vessel surveys typically have a 2-m cross-shore resolution, 25 or 50-m alongshore resolution, and vertical accuracy of 0.05-m. The Coastal Research Amphibious Buggy (CRAB) typically has a 1-m cross-shore resolution, 25 or 50-m alongshore resolution and vertical accuracy of 0.03-m. Survey data is publicly available from the FRF data repository (US Army Corps of Engineers, 2020).

Comparison pre-simulation and post-simulation DEMs from the three periods included in the study revealed offshore sandbar migration. Full surveys were not conducted during the Jan – Feb munitions mobility experiment simulation period, so the background DEM used in the outer grid was used to generate bathymetry for in inner grid. However, a survey conducted on 14 Dec 2014, which was not used to initialize the model, indicated that a sandbar that was relatively uniform in the alongshore direction was was located at ~200 m in the cross-shore coordinate system (Figure 11). The 18 Mar 2015 survey shows the sandbar was located at the cross-shore position of ~265 m and was relatively uniform in the alongshore direction. Note that the surveyed datasets were not used to initialize the model because they were not coincident with simulation period. Instead, the simulation for this period was initialized with the background DEM only. During the Oct 2015 simulation period, a sandbar was located between 200 and 250 m in the cross-shore coordinate (Figure 12). During the passage of the Northeaster storm and Hurricane Joaquin, the sandbar migrated ~50 m offshore over most of the surveyed area, and attached to

the shore between y = 800 m and 875 m to produce a terrace (red accretional area in Figure 12). Two 3- to 4-m deep troughs developed adjacent to the terrace (blue erosional areas north and south of the accretional terrace in Figure 12). Bathymetric observations on 4 Sep 2019 and 9 Sep 2019 bracketed Hurricane Dorian and had the shortest interval between surveys of the three periods in the study. Between the surveys, the sandbar migrated offshore ~15 m.

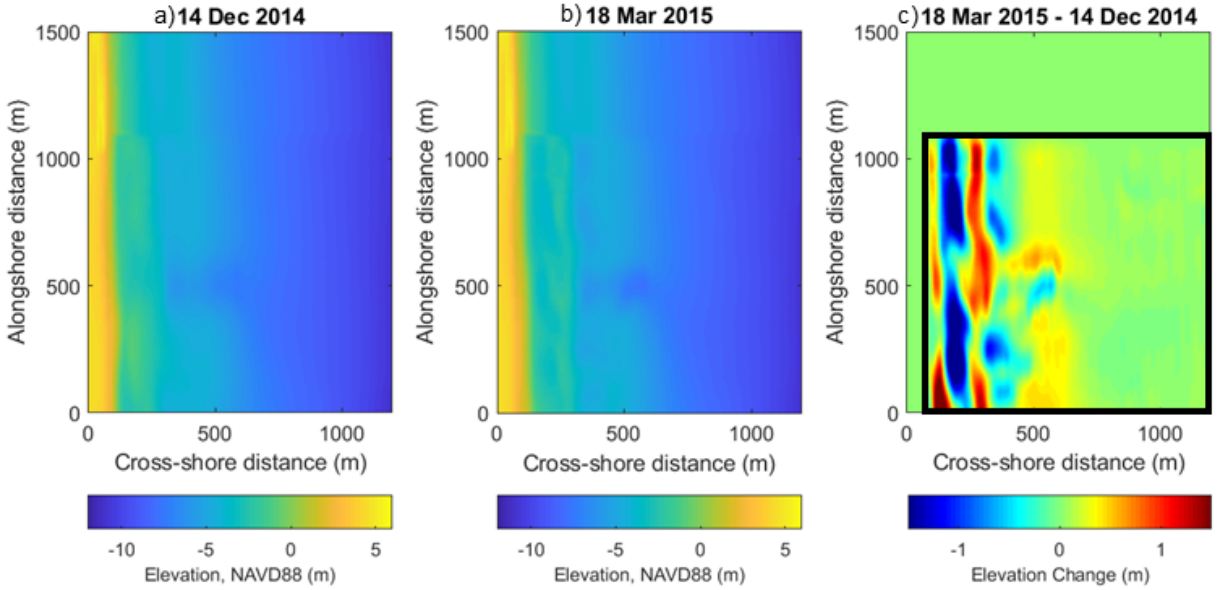

Figure 11. a) Bathymetry datasets created from the background Digital Elevation Model (DEM) and surveyed elevations collected on a) 14 Dec 2014 and b) 18 Mar 2015. c) Elevation change between the two surveyed dates where red represents accretion and blue represents erosion. The area surveyed on both dates is denoted by the black box.

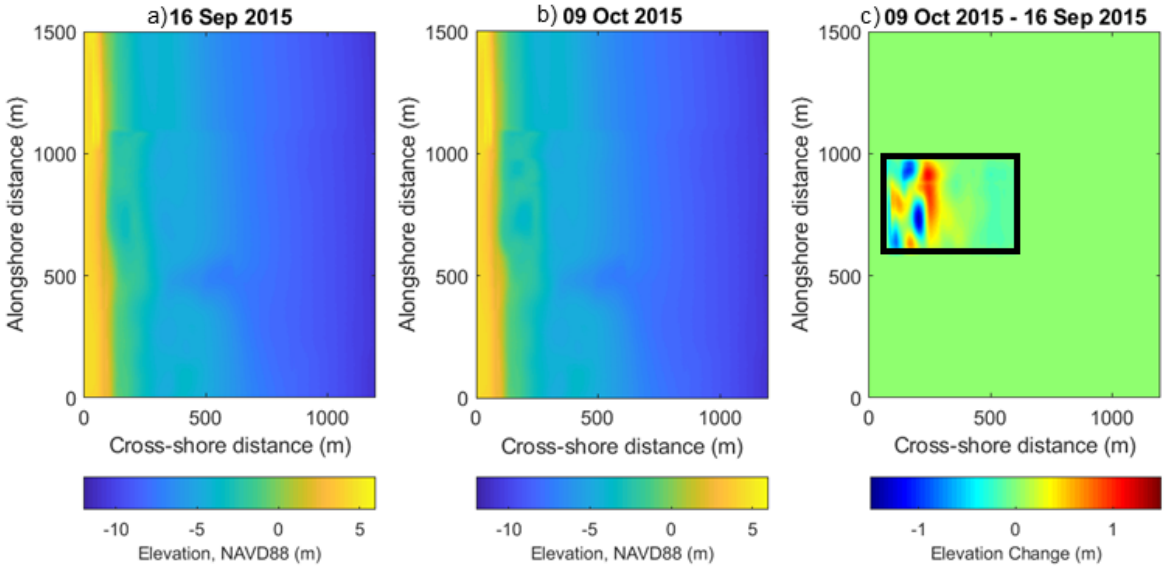

Figure 12. a) The background Digital Elevation Model (DEM) updated with survey data from 16 Sep 2015 was used to initialize model bathymetry for the BathyDuck Experiment simulation. b) The background DEM updated with new survey data from 9 Oct 2015 between alongshore locations of 500 and 1000 m. c) The elevation change between the surveyed dates and areas indicate complex sandbar morphology including development of a terrace near the shoreline with depressions to the north and south of the terrace. The area surveyed on both dates is denoted by the black box.

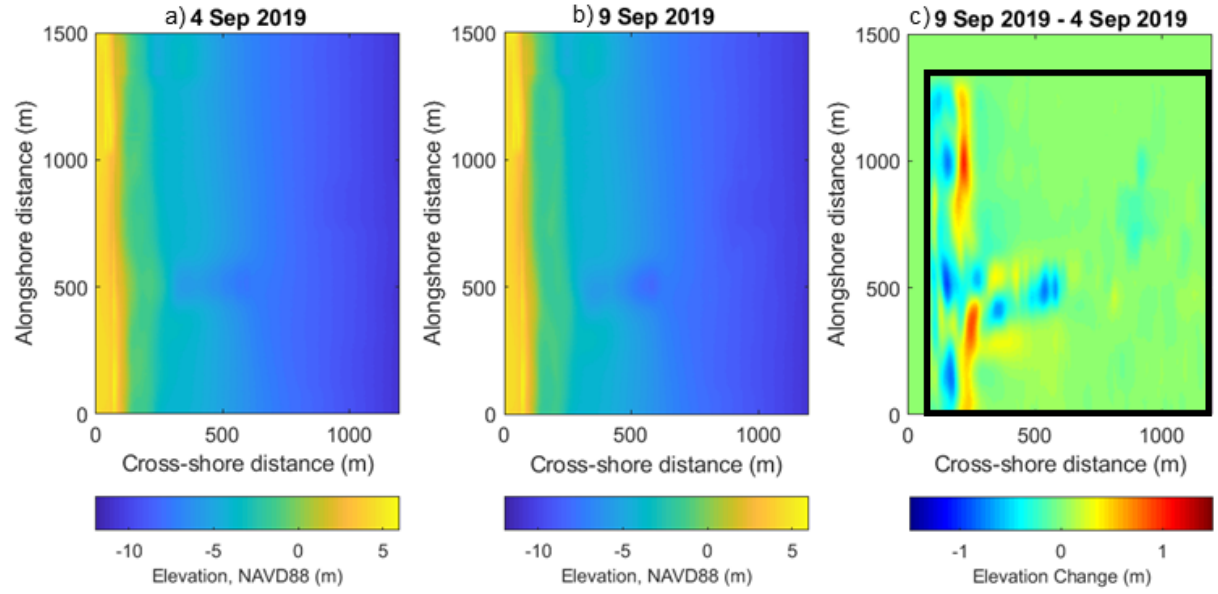

Figure 13. a) The background Digital Elevation Model (DEM) updated with survey data from 3 Sep 2019 was used to initialize model bathymetry for the Hurricane Dorian simulation. b) The background DEM updated with survey data from 9 Sep 2019 between alongshore locations of 0 and 1250 m. c) The elevation changes between the surveyed dates and areas indicate offshore sandbar migration during the passage of Hurricane Dorian.

2.4. Model description

To develop input for UnMES, we performed depth-averaged hydro- and morphodynamic nearshore simulations with Delft3D (Lesser et al., 2004). Delft3D includes a system of coupled models (wave, circulation, and morphology) to simulate the hydrodynamic flow and resulting morphologic change within a model domain. Currents are modeled with the circulation module (FLOW), which solves the non-linear shallow water equations derived from the depth-averaged Navier-Stokes equations (employing the hydrostatic pressure assumption) and the $k - \varepsilon$ turbulence closure model. Simultaneously, the morphological module (MOR) calculates the transport of cohesive and non-cohesive sediment fractions by solving the advection-diffusion equation within the FLOW module. The exchange of sediment between the water column and bed is a function of the sediment settling velocity, bed shear stress, and local sediment pickup function (e.g., Van Rijn, 1993). The subsequent change in bed level is calculated and updated every time step (typically 1-60 sec). Waves are modeled with the third-generation spectral wind wave model SWAN (Booij et al., 1999) and is hereby referred to as WAVE. The WAVE and FLOW simulations are coupled at a user defined coupling time step, typically 30-60 min. At each coupling time step, a WAVE simulation is run with updated depth and current information from FLOW. WAVE then transfers the updated wave field information (RMS wave height, peak spectral period, wave direction, mass fluxes, etc.) back to FLOW, where the effects of the waves on the currents and morphology are calculated. Wave effects included in Delft3D are the wave forcing due to breaking, enhanced bed shear stress, wave-induced mass flux and turbulence production, and streaming. Inputs to Delft3D include initial bathymetry, hydrodynamic and atmospheric boundary conditions (e.g., waves and wind), and sediment grain size.

2.5. Model Setup

The nested simulation setup runs FLOW in a regional US East Coast grid domain that extends from Cape Cod, MA to Charleston, SC (denoted as 'regional'). The regional grid has a 1-km resolution and a total of 795,660 cells (894 x 890). The simulation is forced with modeled winds from the Navy's Coupled Ocean and Atmospheric Mesoscale Prediction System (COAMPS) and modeled tides (TPXO). The regional grid provides current boundary conditions to a nested FLOW outer grid domain that extends 48-km in the along-shore and 18-km in the cross-shore with 100-m resolution and a maximum depth of approximately 26-m (denoted as 'outer'). The outer grid has a total of 81,356 cells (172 x 473). This nested outer grid provides the current boundary conditions for the inner-most coupled wave-circulation-sediment transport simulation domain (denoted as 'inner'). The inner FLOW domain extends 4-km in the along-shore and 2-km in the cross-shore with 10-m resolution and a maximum depth of approximately 11 m. The inner FLOW grid has a total of 50,421 cells (147×343). The inner and outer FLOW domains impose a flow velocity generated from its parent domain on the cross-shore open boundaries (north and south) of the FLOW simulations. A Riemann invariant boundary is used at the seaward (offshore) boundary, which incorporates both the water level and the current normal to the boundary. It's used to simulate a weakly reflective boundary in order to reduce reflections along open boundaries. The inner FLOW simulation domain is coupled to a nested WAVE simulation domain. For the ensemble simulations described in Section 2.6, parameters are varied within the inner WAVE-FLOW domain. A single vertical layer, depth-averaged model setup was used in the FLOW simulations.

The WAVE domain is run on three nested grids at 500-m, 100-m, and 50-m resolutions where the outer grid is driven with the spectral wave observations and the inner-most WAVE domain is two-way coupled with the inner-most FLOW domain (Figure 14 and Figure 15). The outer wave grid extends 18-km offshore to a depth of 26 m and extends 49 km in the alongshore direction. The wave boundary conditions for the north, south, and offshore boundaries of the outer grid were generated from directional wave spectra recorded by a Waverider buoy in 26-m water depth. The outer grid consisted of 3,492 cells (36 × 97) at 500-m resolution. The outer wave grid provides boundary conditions to the middle grid that extends 5.5 km offshore and 13 km in the along-shore consisting of 6,120 cells (51 × 120) at 100-m resolution. The middle wave grid provides boundary conditions to the inner wave grid that extends 2.5 km offshore and 5 km in the along-shore consisting of 2,673 cells (33 × 81) at 50-m resolution. The WAVE simulations are run in stationary mode at the same sampling time as the observations (30 min).

The fully coupled WAVE-FLOW-MOR model is run for the inner domain with a FLOW time step of 2.4 s and a FLOW-WAVE coupling time step of 30 min. An erodible 10-m thick bed composed of non-cohesive quartz sand of grain size 0.2 mm was imposed within the inner domain. Bed roughness is estimated using a Manning's coefficient of 0.02 s $m^{-1/3}$ as the default value, which is typical for nearshore sandy conditions. The friction coefficient was calculated using the Chézy formulation given by,

$$C = \frac{h^{\frac{1}{6}}}{n} \tag{1}$$

where C is the Chézy coefficient, h is the water depth, and n is the Manning's coefficient. In simulations specifying the Manning's coefficient, the bed roughness is dependent on the water depth. The van Rijn sediment transport formulation was used as the default formulation except in the Sep 2019 Hurricane Dorian simulations, where the Soulsby formulation was used. The initial bathymetries for the inner grid WAVE and FLOW simulations are described in Section 2.3.

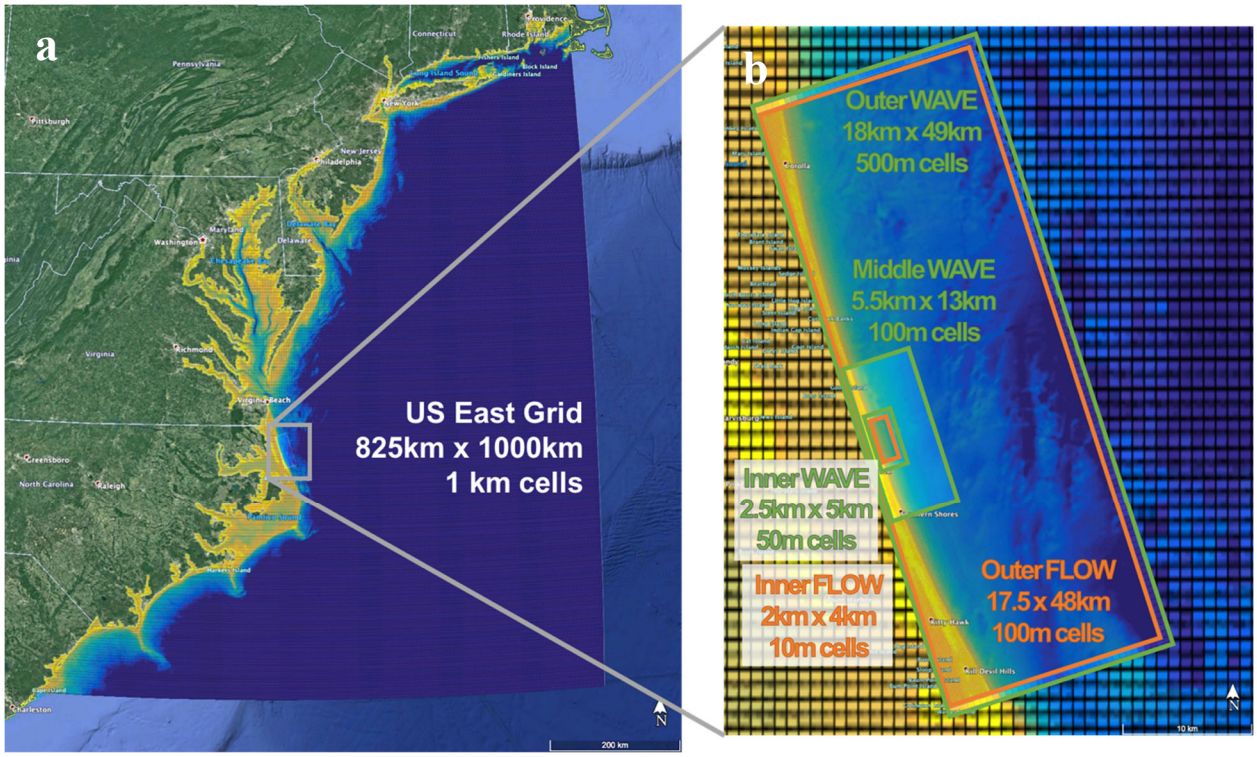

Figure 14. Regional, outer, and inner model domains and grid mesh (black lines) of the FLOW and WAVE simulations with the initial bathymetry contoured in the background. The regional FLOW grid (a) covers most of the Eastern seaboard of the US. The inset (b) shows the higher resolution grids for the FLOW (orange) and WAVE (green) simulations. The initial bathymetry within the inner WAVE and FLOW grids are updated with new surveyed elevations merged into the background DEM for each simulation period (Section 2.3)

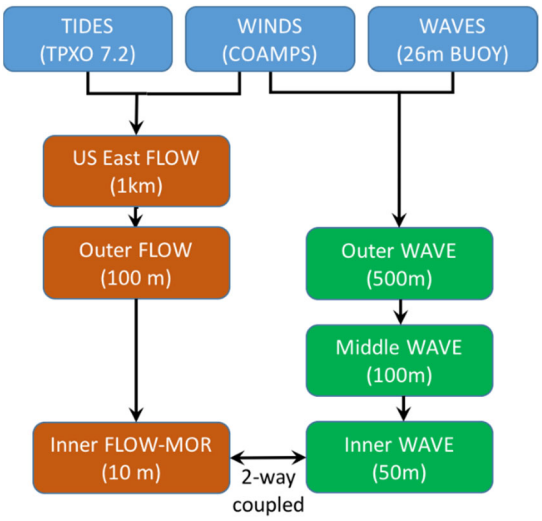

Figure 15. Flow chart of model setup. Blue boxes represent forcing inputs, orange boxes represent FLOW domains and green boxes represent WAVE domains. Horizontally adjacent boxes denote domains of approximately the same size.

2.6. Generalized Likelihood Uncertainty Estimation (GLUE)

In order to assess the model sensitivity, optimize model parameters, and quantify model uncertainty, we adapted the Generalized Likelihood Uncertainty Estimate (GLUE) method for use with Delft3D (Simmons et al., 2017). The GLUE methodology consists of three primary steps: 1) generate model parameters and ranges, 2) run and assign likelihood to model ensemble members, 3) analyze model ensemble members. In the following subsection, we provide a summary of the GLUE method as applied to our study. For a full description of the method as applied to coastal modeling, we refer the reader to Simmons et al. (2017) and the references therein.

We explored three model parameters and four sediment transport formulae described in the Delft3D User's Manual as having the potential for high model sensitivity, and five combinations of wind forcing using the GLUE methodology. Parameter values spanned a reasonable range for the field site and included typically recommended values by Delft3D developers (Table 2 and Table 3). The variations were as follows:

- ST Form – The set of deterministic equations to calculate the magnitude and direction of sediment suspended and transported by the flow
- Ccofu – Manning's friction coefficient describes the resistance to flow due to bottom roughness
- Vicouv – horizontal eddy viscosity (m^2/s) defines the magnitude of the background horizontal flow velocity motions
- Dicouv – horizontal eddy diffusivity (m^2/s) defines the magnitude of the background sediment diffusion
- Wind – the type of wind forcing that ultimately transfers momentum to the surface waves and currents

The value ranges of the model coefficients and the formulations for the first four variations are given in Table 2 with the model defaults highlighted in gray. The sediment transport formulations chosen include those only incorporating both wave and current forcing and that are recommended for coastal

applications. The other coefficient values span the ranges that are stated in the Delft3D manual. The wind forcing variations are described in Table 3. The winds forced in the simulations are obtained through both models and observations. The observed winds are provided by a meteorological station at the end of the FRF pier. The modeled winds are provided by the Coupled Ocean Atmospheric Mesoscale Prediction System (COAMPS), the Navy's operational regional scale atmospheric model. The model typically underpredicts wind speed near the coast and during storms; therefore, an additional wind forcing variation includes a parameterized hurricane wind field merged with the COAMPS simulated wind field. To address the underestimation of the modeled winds near the coast, some simulations were forced with the modeled winds in the regional grid and the observed winds in the nearshore grids. Another wind forcing variation includes a different wind stress formulation that determines the amount of wind shear stress imposed on the ocean surface.

Table 2. Values of the model coefficients and sediment transport formulations used for GLUE analysis

Variable	**Description**	**Units**	**lower range**		**DEFAULT**	**higher range**		
ST Form	Sed trans formulation	(-)	Bijker	van Rijn		Soulsby	SvR	
Ccofu	Manning's coefficient	(-)		0.01	0.02	0.025	0.03	0.04
Vicouv	Horiz eddy viscosity	m^2/s	0.10	0.50	1.00	2.00	5.00	
Dicouv	Horiz eddy diffusivity	m^2/s	0.01	0.05	0.10	0.20	0.50	

Table 3. Description of varying wind forcing used for GLUE analysis

Regional Grid	**Outer Grid**	**Inner Grid**
COAMPS	No wind	No wind
COAMPS	Observations at FRF Pier	Observations at FRF Pier
Observations at FRF Pier	Observations at FRF Pier	Observations at FRF Pier
COAMPS	Observations at FRF Pier with modified wind stress	Observations at FRF Pier with modified wind stress
COAMPS plus parameterized hurricane winds	Observations at FRF Pier	Observations at FRF Pier

The second step of the GLUE method is to quantify the likelihood of each ensemble member being the optimal parameterization based on the model skill, *S*. In GLUE, *S* must be zero for all cases deemed 'non-behavioral' (i.e., produce results that have no skill). *S* must increase monotonically for cases that reasonably reproduce observations. We defined *S* by adapting the classification system of van Rijn et al. (2003). In the adapted van Rijn et al. (2003) system, hydrodynamic model performance is assessed non-dimensionally, using the relative mean absolute error, *RMAE*, between wave and flow simulations, x_m, and observations, x_o,

$$RMAE = 1 - \langle |\chi_m - \chi_o| - \Delta\chi_m \rangle / \langle \chi_o \rangle, \quad (2)$$

where the subscript m denotes the model and o denotes the observations, $\Delta\chi_m$ describes the measurement error, and angled brackets indicate the temporal mean. *RMAE* is less susceptible to outliers than the *RMSD* (van Rijn et al., 2003). Depth-averaged current velocity observations at the 6 and 11-m current profilers were compared with the depth-averaged FLOW simulations in the analysis in (2).

The Brier Skill Score, *BSS*, was used to quantify the difference between morphodynamic simulation results and the surveyed bathymetry. For morphological models, *BSS* is defined as

$$BSS = 1 - \frac{\sum_{j=1}^{N}(|z_m - z_o|)^2}{\sum_{j=1}^{N}(z_i - z_o)^2} \quad , \tag{3}$$

where z_m is the modeled bed elevation at the end simulation period, z_o is the observed bed elevation at the end of the simulation period, and z_i is the initial bed elevation. Simulations that perfectly reproduce the observed change in bed elevation have a *BSS* of 1. Simulations that under-estimate the observed bed elevation change have a BSS between 0 and 1. Simulations that over-estimate the observed change in bed elevation have a BBS of less than 0.

We used the measures of *S* along with a behavioral/non-behavioral threshold to define the likelihood of each ensemble member. As suggested by Simmons et al. (2017), we used a threshold value to define the cutoff between 'behavioral' and 'non-behavioral' ensemble members. Specifically, we defined threshold values of 0 as the transition. Model skill for ensemble members below the threshold values were set to 0. We defined the likelihood of an ensemble member as

$$L_S = \frac{S_i}{\sum_{i=1}^{n} S_i}, \tag{4}$$

where n is the total number of behavioral WAVE, FLOW, or MOR ensemble members and S_i is the skill of each ensemble member.

The final step of the GLUE method is to analyze model ensemble members in terms of quantifying model sensitivity, optimizing model parameters, and quantifying model uncertainty. To assess model sensitivity to parameters, we plotted the cumulative likelihood measure, L_s, distribution. The difference between the cumulative likelihood distribution and a distribution where each parameter value in the sample space is assigned equal probablity gives an indication of model sensitivity to a parameter. We quantified sensitivity using the Kolmogorov-Smirnov D statistic, which describes the maximum distance between the cumulative likelihood distribution and the equal probabilty distribution. The D statistic has extreme values of 0 and 1. 0 indicates an insensitive parameter and 1 characterizes a highly sensitive parameter. These values were used to rank each of parameters investigated. We optimized model parameters by calculating the posterior distributions from the likely values associated with the ensemble members for each parameter range.

2.7. Unexploded Munitions Expert System (UnMES)

A Bayesian Network is a probabilistic machine learning model that represents the causal relationship between variables (Pearl, 1988). Bayesian networks are often represented qualitatively as a directed acyclic graph where boxes, known as nodes, represent the variables in the network; arrows, known as arcs, represent the conditional probabilities between variables; and the direction of the arcs indicates causality (Charniak, 1991). Parent nodes are independent variables, with no incoming arrows. Child nodes are dependent on one or more parent nodes. Once trained, Bayesian networks may be supplied with new information to update the probability distributions within the network using Bayesian inference. Bayesian networks are appropriate to use in modeling situations where data or complete understanding of

the process modeled is not fully known, as is the case with munitions mobility and burial (Aguilera et al., 2011).

The Unexploded Munitions Expert System (UnMES) is a Bayesian Network developed as part of MR-2645 and MR-2227, to quantify our understanding of the behavior of munitions mobility and burial (Figure 16). UnMES was built with the commercial Bayesian Network software, Netica (Norsys Software Corporation, 2011). The structure of the causal relationships described by the schematic drawing in Figure 16 was defined by the developers of UnMES. Boxes in Figure 16 represent the variables that comprise the network and arrows represent the causal relationships defined by the conditional probability between connected variables. Boxes in bold outline are input in the coupled Delft3D-UnMES implementation. Hydrodynamic and morphodynamic variables are colored cyan; intermediate variables, which may be calculated directly in UnMES or supplied directly from post-processed Delft3D results are colored beige; variables describing UXOs are colored red; output variables describing munitions mobility are colored green; and the output variable describing munitions burial is colored dark pink. UnMES was trained with simple, physics-based formulations to quantify the conditional probabilities between variables (see MR-2645 for more details). Updated probability distributions are estimated given the new information using Bayesian inference. In the implementation in the present study, updated information about hydrodynamics and morphodynamics are defined by Delft3D simulations.

Our coupled implementation of Delft3D/UnMES consists of three steps. Hydrodynamic and morphodynamic conditions are simulated in Delft3D and post-processed with MATLAB to generate an input file for Netica. Wave heights, periods, directions, and bottom orbital velocities from the inner WAVE grid (Section 2.5) were interpolated on to the higher resolution inner FLOW grid. Bottom velocities, U_b, were estimated from the depth-averaged currents, U_c, as

$$U_b = U_c \kappa / \ln\left(\frac{h}{D_{UXO}}\right), \tag{5}$$

where κ is the von Karman constant,0.41, h is the water depth in meters, and D_{UXO} is the diameter of the UXO in meters. Combined wave and current bottom velocities, U_m, were calculated as

$$U_m = \left(U_w^2 + U_b^2 + 2U_w U_b \cos\beta\right)^{1/2}, \tag{6}$$

where U_w is the bottom orbital velocity, and β is the angle between waves and currents.

The input file for UnMES consists of column of input variables along with other variables included as metadata or for visualization (e.g., Table 3). Each row in the input file represents a cell within the inner FLOW grid. We are presently in the process of converting the post-processing of Delft3D in MATLAB to Python, so that it may be more seamlessly conducted within a high-performance computing architecture. The input file from the post-processing step is used to update UnMES using a Python wrapper with the Netica-C Application Programming Interface (API) described in Section 2.8. Updated estimates of munitions migration distance, migration direction, and burial are produced at each cell within the inner FLOW grid. The updated estimates are saved in a Keyhole Markup language Zipped (KMZ) file for visualizing the results in a geo-viewer (e.g., Google Earth).

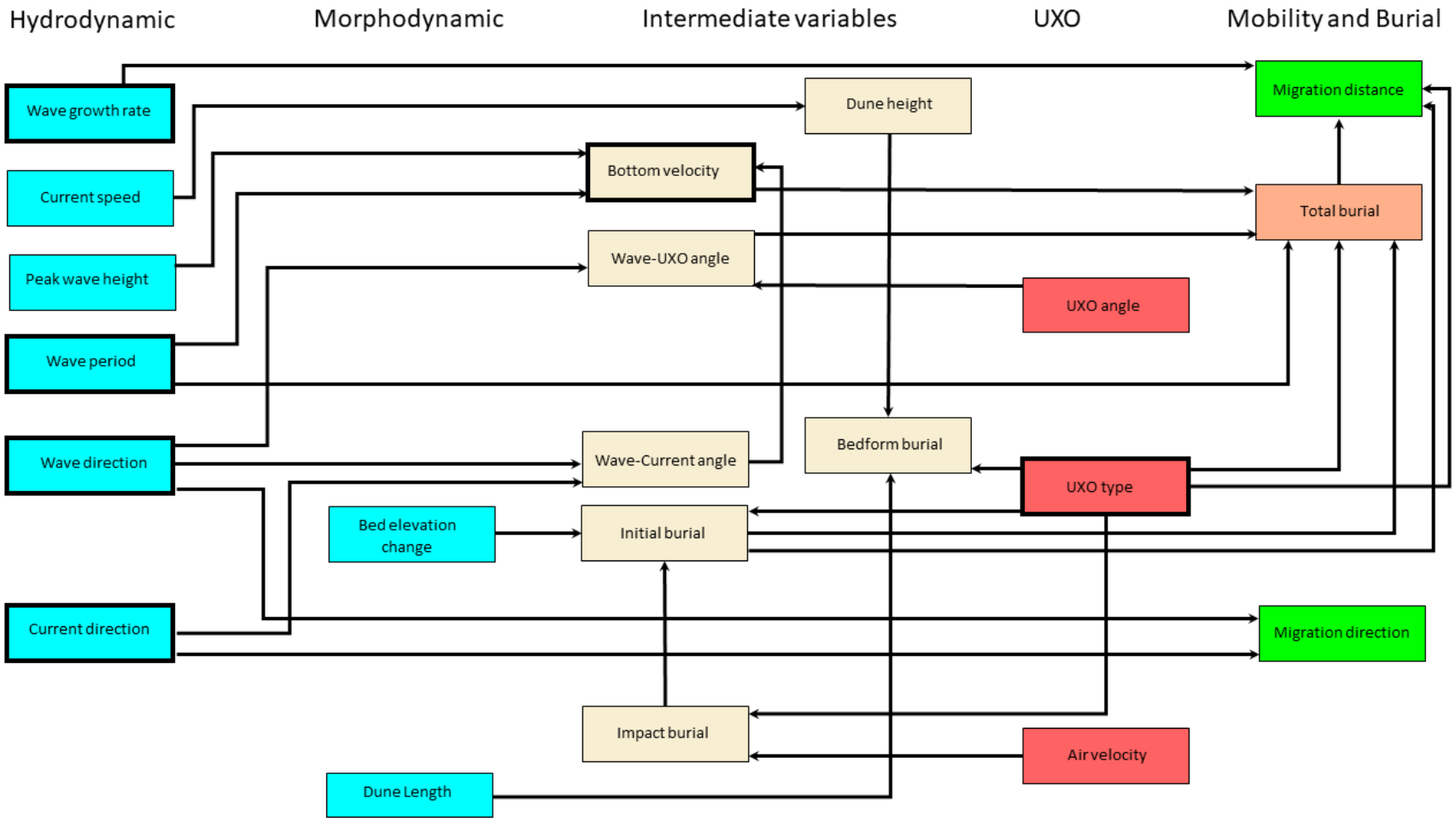

Figure 16. Schematic diagram of the Unexploded Munitions Expert System (UnMES) Bayesian network developed in MR-2645 and 2777.

Table 4. Several lines from an example input file to define updated variables for UnMES during the peak of the Northeaster at 0830 11 February 2015.

ind	t_datenum	lon	lat	h_m	Hsig	T	wDir	Uc	cDir	XDir	YDir	Um	beta	UXO	TB	Mdist	Mdir
25	736006.3660	-75.745522	36.174389	-4.32	2.51	11.9	-4.06	0.39	-69	0.38	0.02	1.14	65	8.1	*	*	*
26	736006.3660	-75.745417	36.174417	-4.44	2.54	11.9	-4.05	0.40	-71	0.38	0.01	1.13	67	8.1	*	*	*
27	736006.3660	-75.745311	36.174445	-4.52	2.57	11.9	-4.03	0.42	-72	0.37	0.00	1.13	68	8.1	*	*	*
28	736006.3660	-75.745206	36.174473	-4.58	2.60	11.9	-4.02	0.44	-74	0.37	-0.01	1.13	70	8.1	*	*	*

*Column headers are given as abbreviated input for Netica: ind (index in file, included as metadata), t_datenum (time of Delft3D output, included as metadata), lon (longitude of Delft3D inner FLOW grid cell, included for visualization), lat (latitude of Delft3D inner FLOW grid cell, included for visualization), h_m (elevation of Delft3D grid cell in m relative to NAVD88, included for visualization), Hsig (significant wave height in m, included for visualization), T (peak period in s), wDir (wave direction in shore normal FRF coordinate system used in UnMES), Uc (current speed in m/s, included for visualization), cDir (current direction in shore normal FRF coordinate system used in UnMES), XDir (X-component of current velocity relative to true north, included for visualizing current), YDir (Y-component of current velocity relative to true north, included for visualizing current), Um (combined wave and current near bottom velocity in m/s assuming a log profile for currents), beta (angle between waves and currents), UXO (flag for UXO type), TB (placeholder for total burial output), Mdist(placeholder in m for migration distance output), Mdir (placeholder for migration direction output). Variables with no data are represented as an asterisk in Netica input files.

2.8. Linking Delft3D and UnMES

The goal of MR2733 is to update UnMES with Delft3D simulations in order to produce cartographic visualizations of the probability of munitions mobility and burial (Figure 1). In the third year of the project, we developed Python code to post-process Delft3D simulations, feed the results to UnMES, and produce visualizations of munitions behavior. The following section is a step-by-step guide to setting up and running the code. The code requires installation of Python 3.7.3 or higher, the capability to compile C++ code within Python, and a geo-viewer to plot KMZ files (e.g., Google Earth).

Setup process:

1. Install C++ compiler using Windows Visual studio v14 (need admin privileges)
2. Open your Anaconda Prompt
3. (Optional) set up a new environment: conda create --name *yourEnvName*
4. (Optional) Activate your environment: conda activate *yourEnvName*
5. If you create a new environment, check to make sure that it has scipy installed
6. Install cython at Anaconda command prompt: conda install -c anaconda cython
7. Check to see if cython/c compiler installed correctly: http://docs.cython.org/en/latest/src/tutorial/cython_tutorial.html#cython-hello-world
8. Install pynetica at the Anaconda command prompt:
    a. Change to the directory where the pynetica package is saved
    b. python setup.py install or python setup.py build_ext –inplace
    c. Check to make sure pynetica was installed: type help('modules') at command prompt and you should see that pynetica is one of the packages installed
9. Make sure you can access Netica from Python by copying Netica.dll and Netica.lib files to your environment (e.g., C:\Users\username\AppData\Local\Continuum\anaconda3\envs\pynetica_test\Lib\site-packages)
10. Make sure you have installed all the other packages you need that don't come with Anaconda:
    a. conda install –c conda-forge simplekml
    b. conda install –c conda-forge palettable
    c. conda install scipy
    d. conda install -c anaconda matplotlib
    e. conda install yaml

Create a casefile in MATLAB (this will be incorporated in python code eventually)

1. Edit and run: C:\Users\mpalmsten\Documents\MATLAB\Delft3D\MATLAB\make_network_input_D3D_jan_mar2015.m

Running UnMES from python using D3D results:

1. Make any changes to DuckEstimates*.py necessary (this should be updated so they are not hard-coded):
    a. Line 39: .neta file name
    b. Line 258-260: case file name
    c. Line 263-266: output location and kmz file name
    d. Lines 90-292: change size of grid if necessary – hard coded for FRF inner grid

3. Results

3.1. Generalized Likelihood Uncertainty Estimation (GLUE)

The sensitivity of the model to the five varying inputs (three coefficients, one set of formulations, one forcing condition) were explored in the GLUE analysis for the October 2015 simulation period (Section 2.6). Here, we describe results of the hydrodynamic analysis followed by results of the sediment transport analysis. Model results for depth-averaged current speed were insensitive to Manning's coefficient (Figure 17 and Figure 18). The Manning's coefficients tested were representative of a smooth bed (0.01) to a cobbled bed (0.04). The K-S D statistic for the Manning's coefficient was 0 for both the 6-m and 11-m locations. Depth-averaged currents were only slightly sensitive to the four sediment transport formulations tested at both water depths (Figure 19 and Figure 20). Modeled depth-averaged currents displayed a small amount of sensitivity to horizontal eddy viscosity but not to the diffusivity coefficients (Figure 21, Figure 22, and Figure 23, Figure 24). These two coefficients define the behavior of eddies and horizontal motions that are not resolved at the horizonal grid resolution. The range of coefficients tested spanned a physically reasonable range. Sensitivity to the variability in all the parameters was similar in both the 6-m and 11-m water depths, with a slightly higher sensitivity at the 6-m depth likely due to the greater interaction of the waves and currents with the bottom. Figure 25 and Figure 26 summarize the hydrodynamic sensitivity of the coefficients and parameterizations. Depth-averaged current magnitudes were most sensitive to the coefficients for horizontal eddy viscosity and the sediment transport formulations.

In addition to model coefficients and formulations, we tested sensitivity of model results to various combinations of wind forcing (Table 3) during Hurricane Dorian in Sep 2019. Modeled depth-averaged currents at the 6-m and 11-m locations exhibited a sensitivity to wind forcing (Figure 27 and Figure 28). Comparison of the K-S D statistic for wind forcing with K-S D statistics for model coefficients and sediment transport formulations revealed that depth-averaged currents were more sensitive to wind forcing than to variations in model parameterizations and sediment transport formulations. Further analysis of the depth-averaged current timeseries demonstrated that results were insensitive to wind forcing during low wind periods, but highly sensitive during the passage of the storm (Figure 29).

An additional GLUE analysis was conducted for the sediment transport formulation with regards to simulated changes in the bathymetry (Figure 30). Note that due to lack of survey data at the beginning of the simulation period, the model was initialized on 3 Oct 2015 with bathymetry collected on 16 Sep 2015, which likely introduces some error in initial depth. The BSS for three of the four sediment transport formulations was negative, indicating that the modeled variability was larger than observed variability. The Soulsby formulation was the only formulation to produce a positive BSS. Cumulative likelihood and K-S D statistics were not calculated because of negative BSS values, making the simulations non-behavioral. However, the range of BSS values qualitatively indicates that the simulated bathymetric change is sensitive to the applied sediment transport formulation.

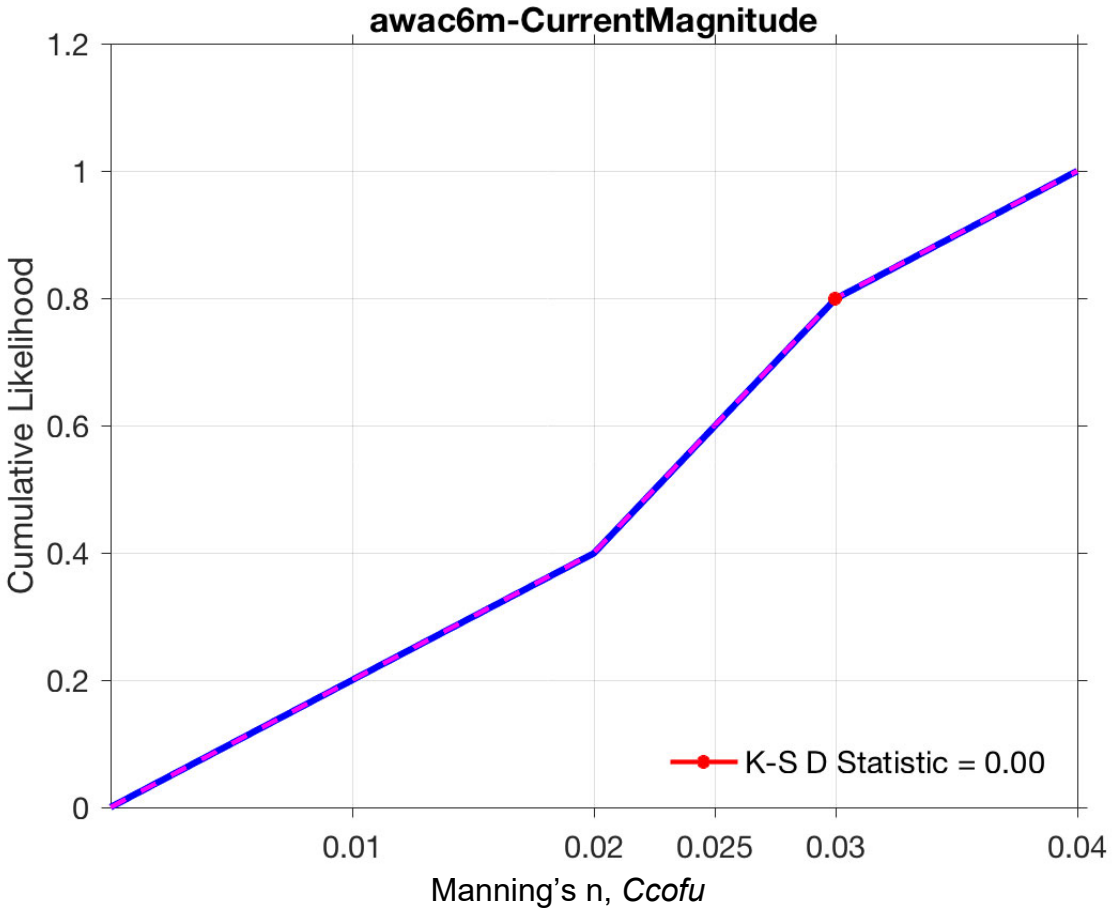

Figure 17. Cumulative likelihood distribution (blue line) and a cumulative distribution where each parameter value is assigned equal probability (magenta dashed line) for Manning's coefficients ranging from 0.01 (representative of a smooth bed) to 0.04 (representative of a cobble bed) at the 6-m wave and current profiler (AWAC). Location of the 6-m AWAC is presented in Figure 9.

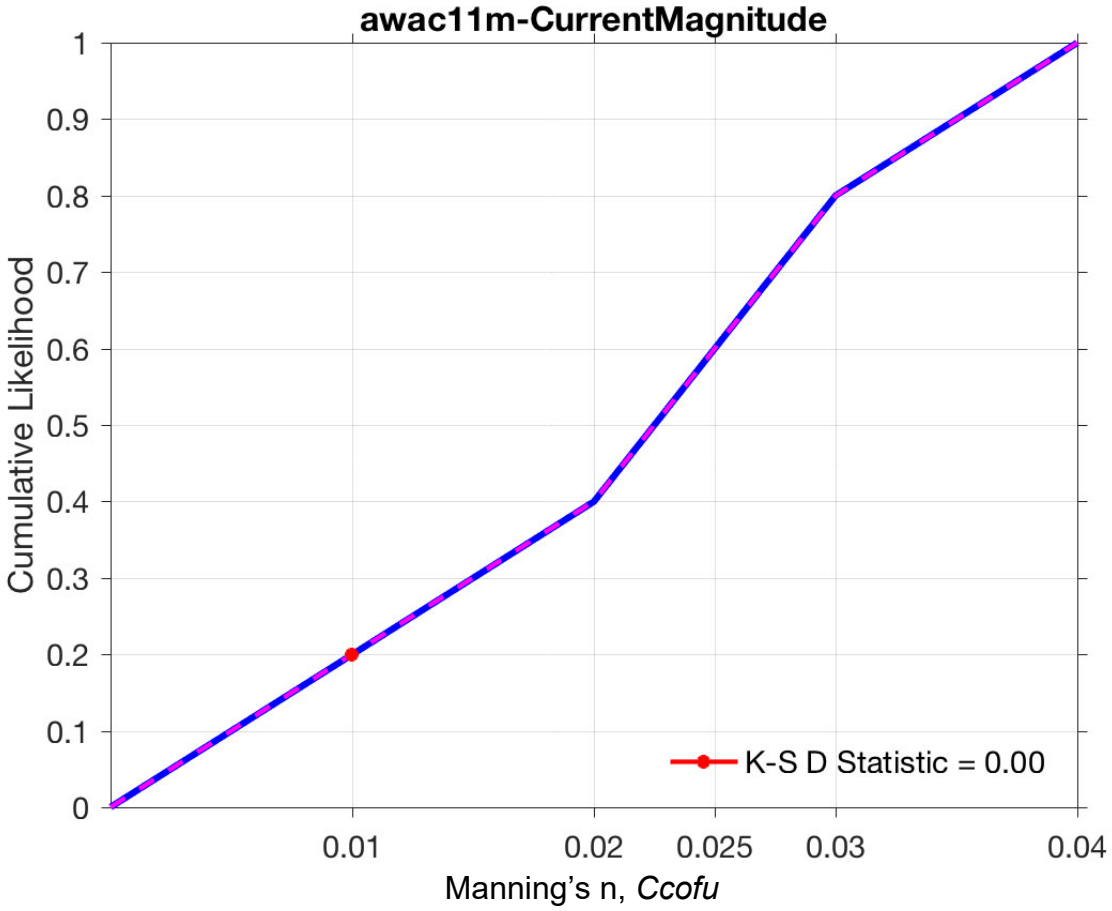

Figure 18. Cumulative likelihood distribution (blue line) and a cumulative distribution where each parameter value is assigned equal probability (magenta dashed line) for Manning's coefficients ranging from 0.01 (representative of a smooth bed) to 0.04 (representative of a cobble bed) at the 11-m wave and current profiler (AWAC). Location of the 11-m AWAC is presented in Figure 9.

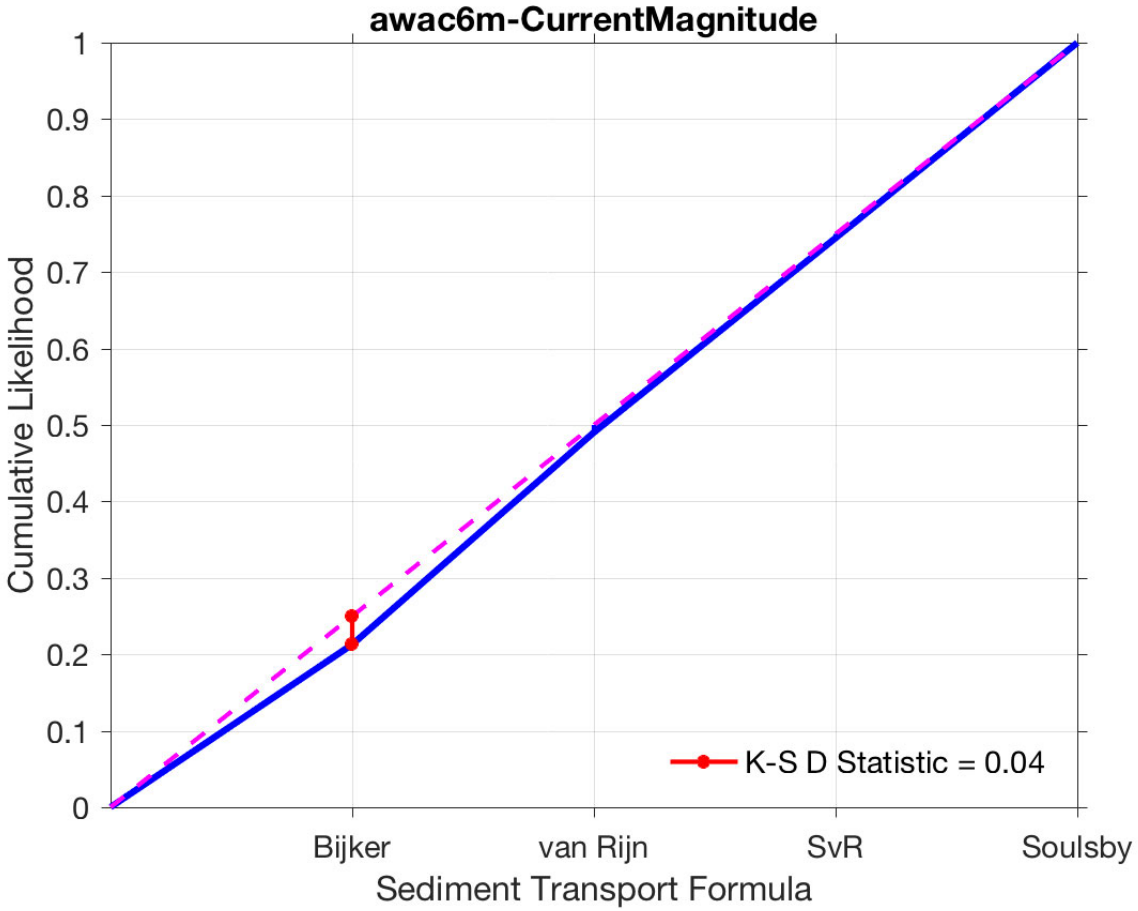

Figure 19. Cumulative likelihood distribution (blue line) and a cumulative distribution where each parameter value is assigned equal probability (magenta dashed line) for the sediment transport formulations. The K-S D statistic indicates that the depth-averaged current speed at this location is only slightly sensitive to the applied sediment transport formulation.

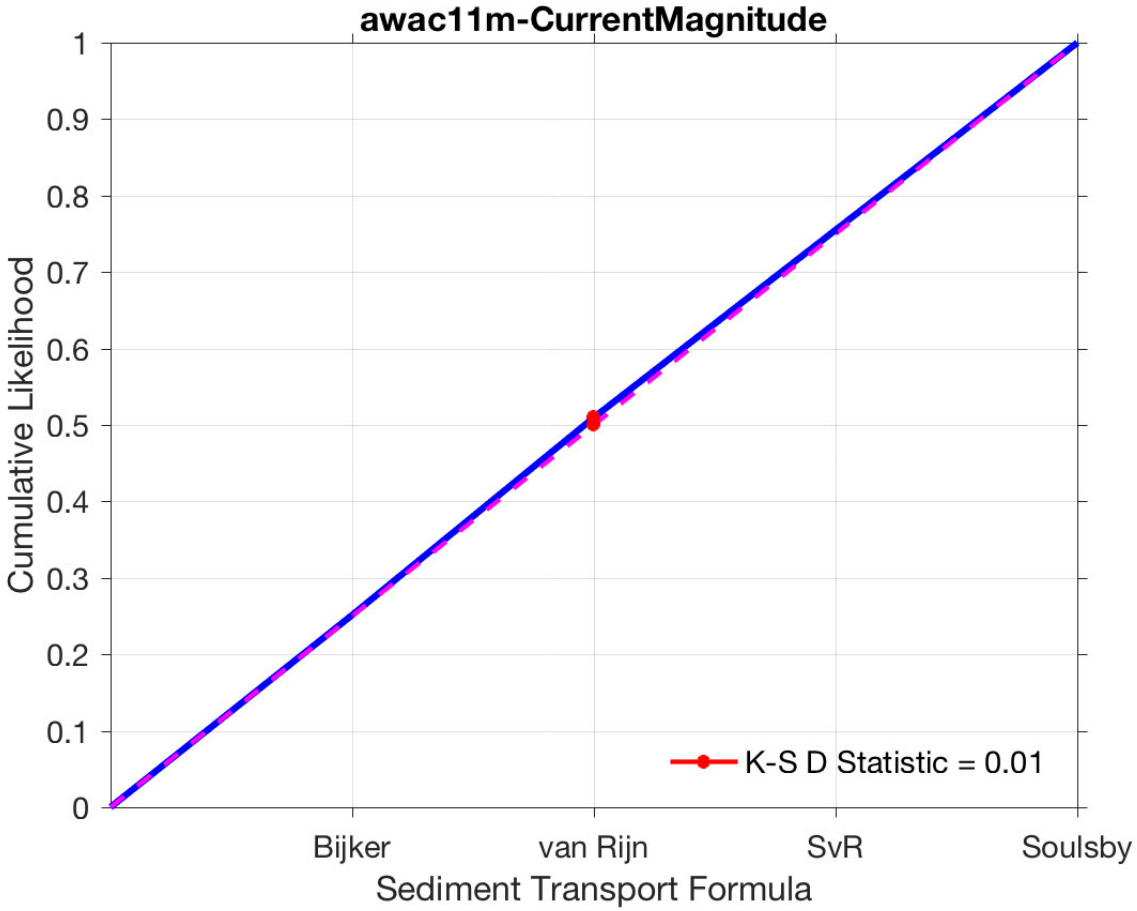

Figure 20. Cumulative likelihood distribution (blue line) and a cumulative distribution where each parameter value is assigned equal probability (magenta dashed line) for the sediment transport formulations.

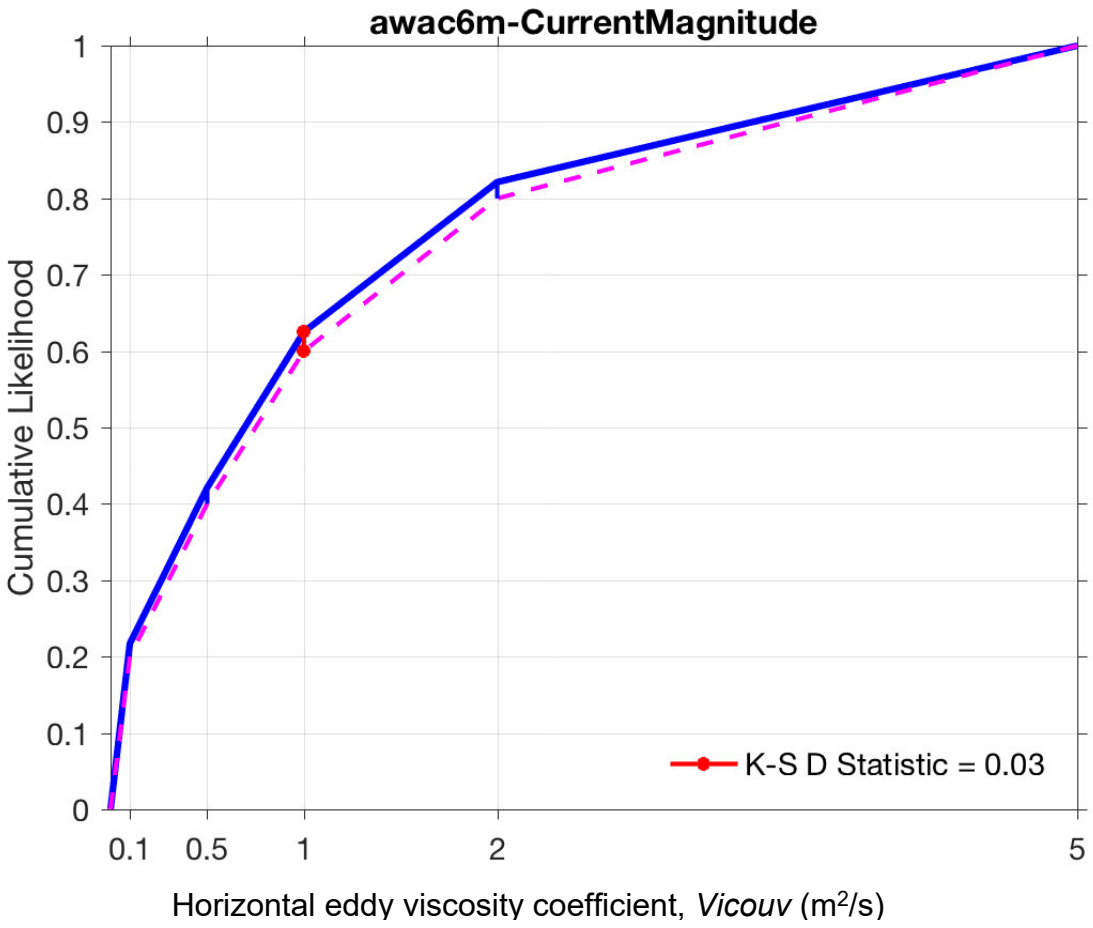

Figure 21. Cumulative likelihood distribution (blue line) and a cumulative distribution where each parameter value is assigned equal probability (magenta dashed line) for the horizontal eddy viscosity coefficient, Vicouv, which parametrizes flow eddies and horizontal motions that are not resolved at the horizonal grid resolution.

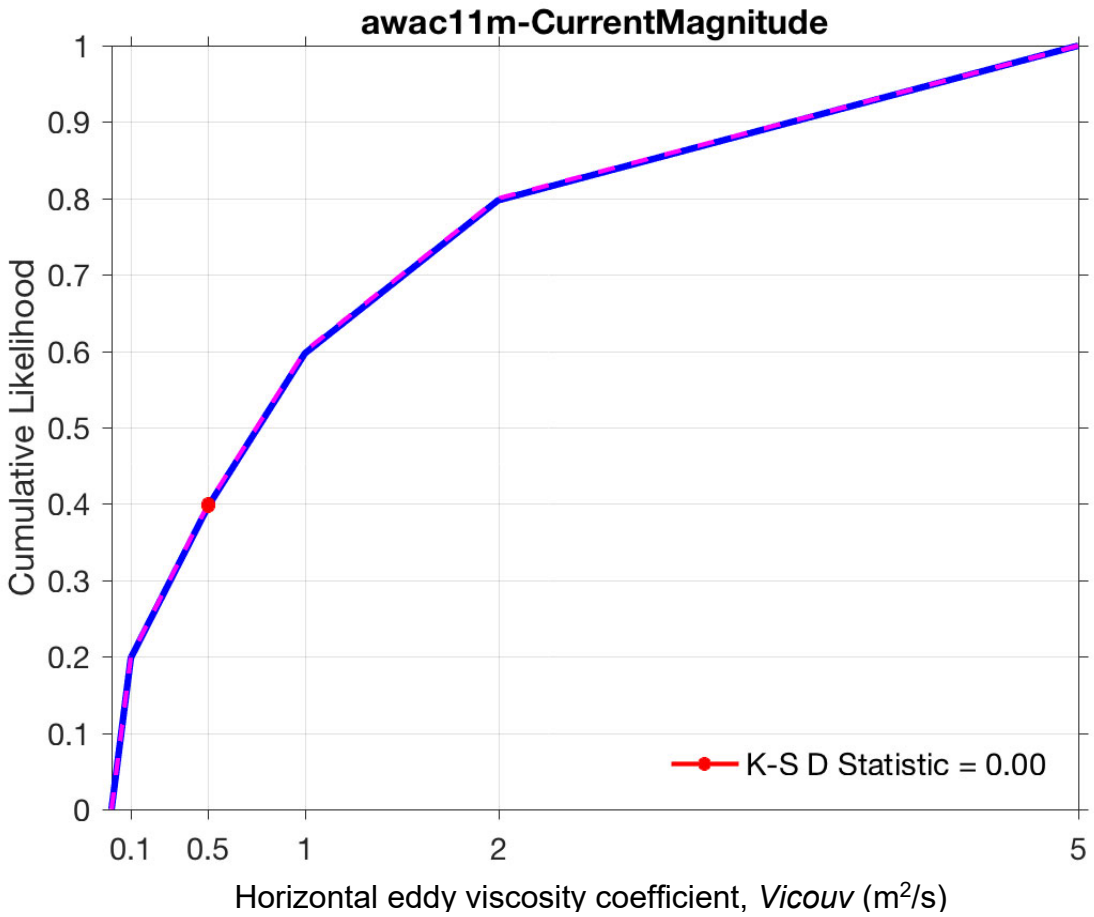

Figure 22. Cumulative likelihood distribution (blue line) and a cumulative distribution where each parameter value is assigned equal probability (magenta dashed line) for the horizontal eddy viscosity coefficient, Vicouv, which parametrizes eddies and horizontal motions that are not resolved at the horizonal grid resolution.

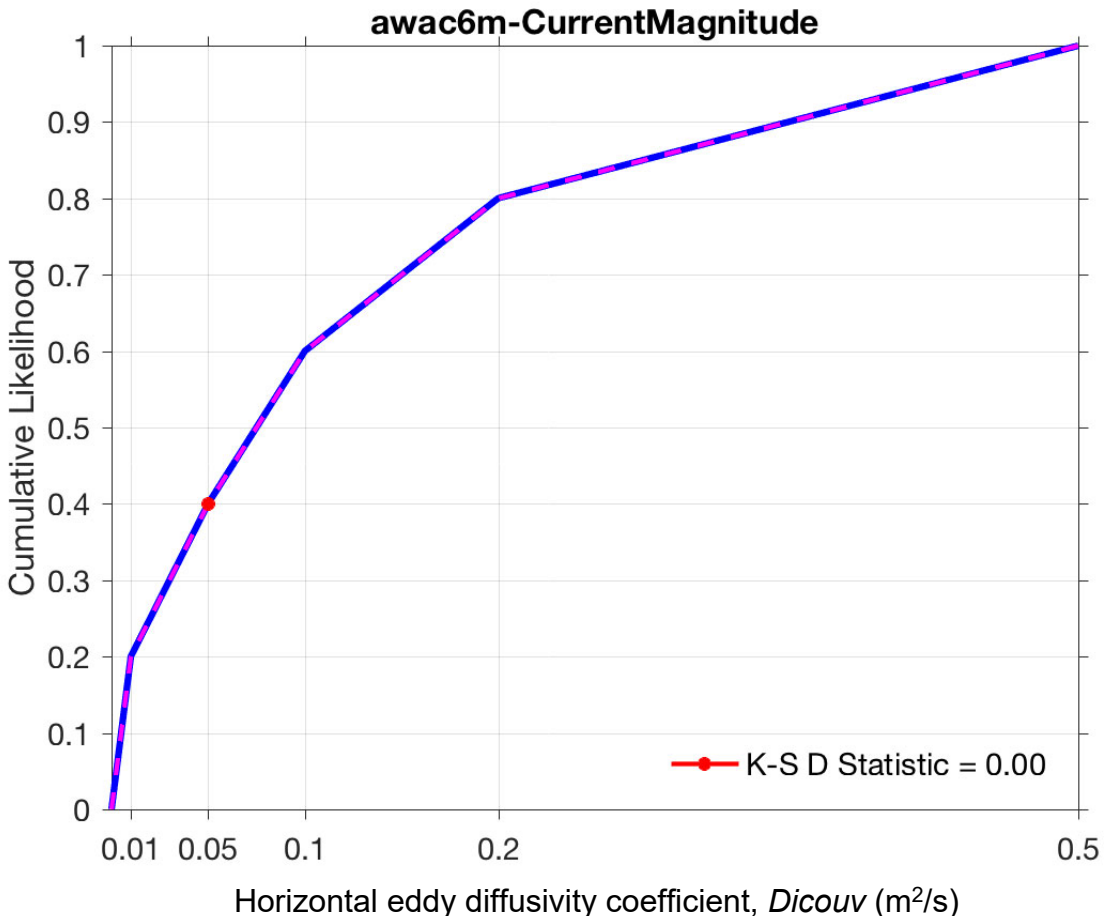

Figure 23. Cumulative likelihood distribution (blue line) and a cumulative distribution where each parameter value is assigned equal probability (magenta dashed line) for the horizontal eddy diffusivity coefficient, Dicouv, which parametrizes the horizontal diffusion of the suspended sediment that is not resolved at the horizonal grid resolution.

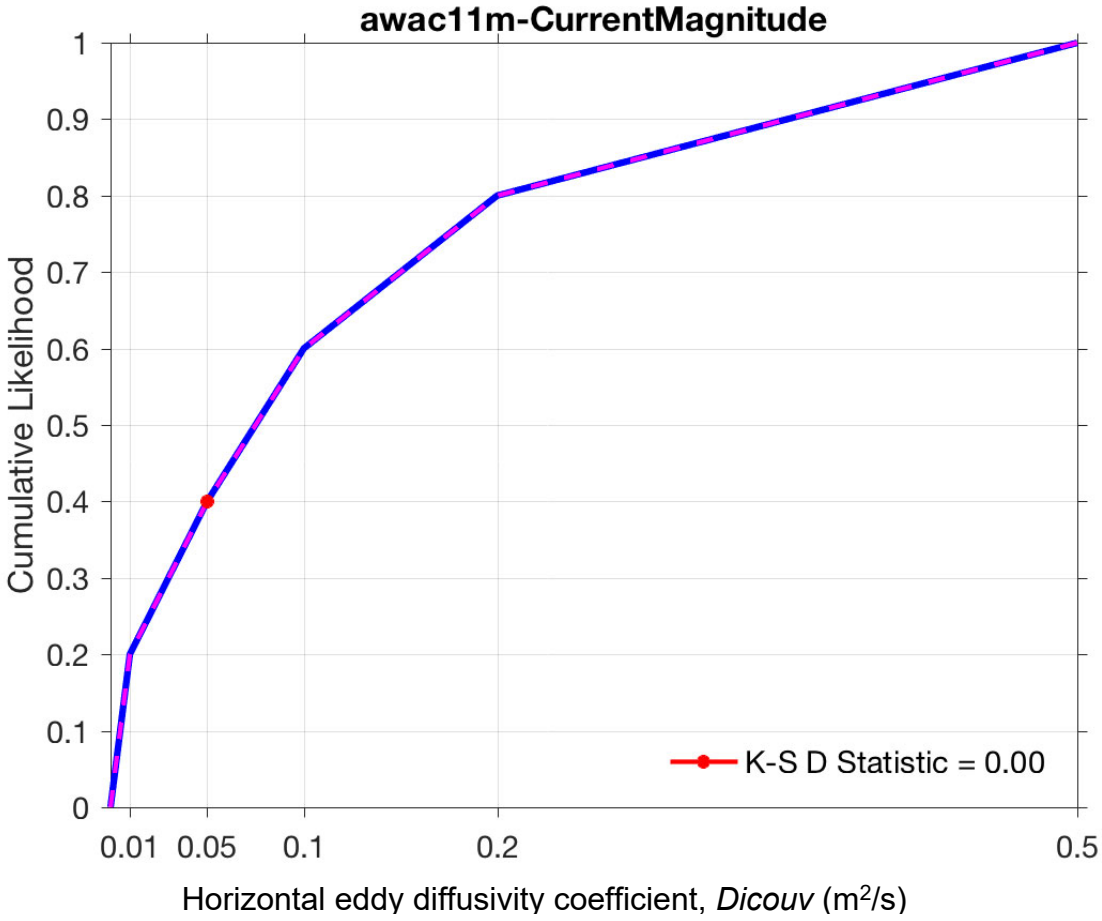

Figure 24. Cumulative likelihood distribution (blue line) and a cumulative distribution where each parameter value is assigned equal probability (magenta dashed line) for the horizontal eddy diffusivity coefficient, Dicouv, which represents the horizontal diffusion of the suspended sediment that is not resolved at the horizonal grid resolution.

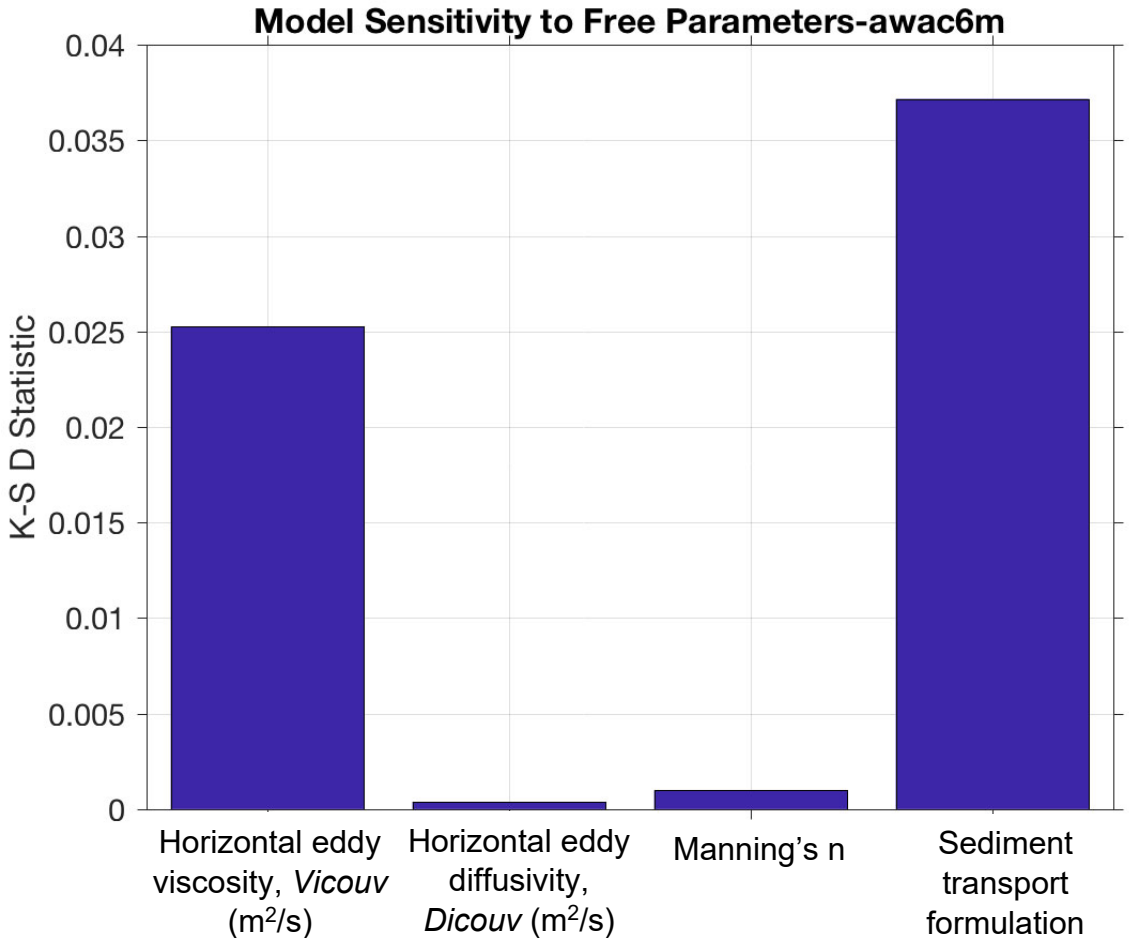

Figure 25. Modeled depth-averaged currents at 6-m water depth exhibited a very low sensitivity to variations in the model coefficients and formulations tested, as the K-S D statistic was near 0 in all cases. Note that K-S D values reported in Figures 17 – 24 are rounded.

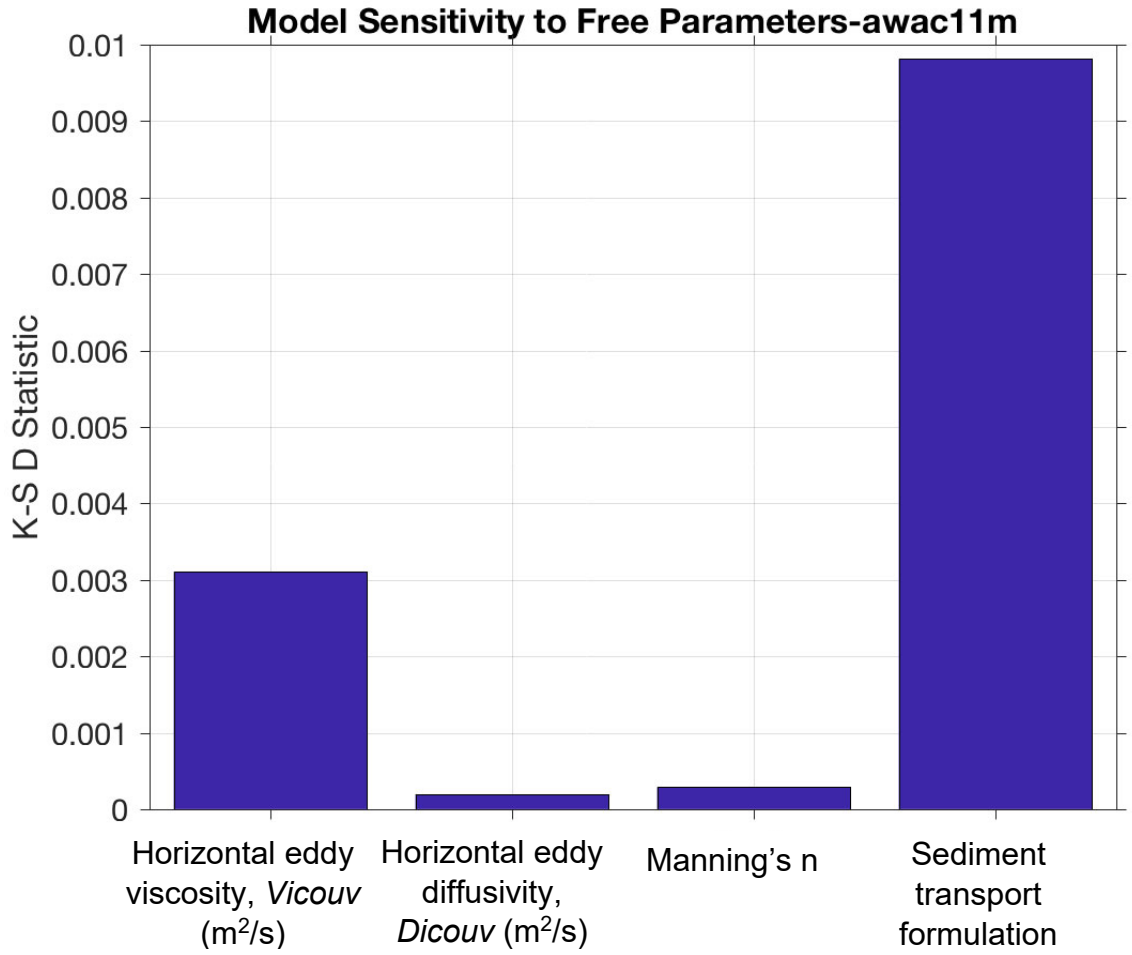

Figure 26. Modeled depth-averaged currents at 11-m water depth exhibited a very low sensitivity to variations in the model coefficients and formulations tested, as the K-S D statistic was near 0 in all cases. Note that K-S D values reported in Figures 17 – 24 are rounded.

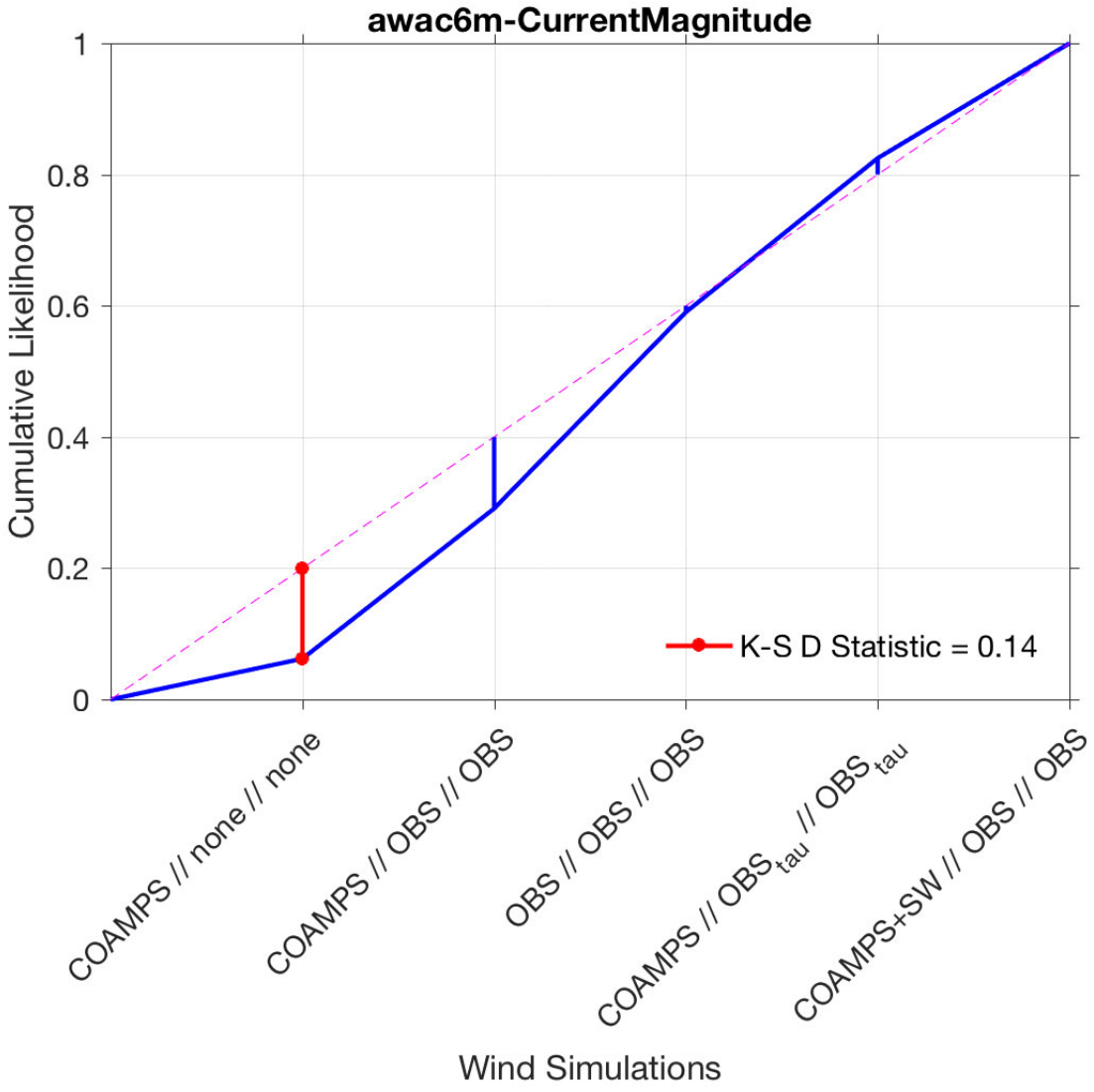

Figure 27. Cumulative likelihood distribution (blue line) and cumulative distribution where each parameter value is assigned equal probability (magenta dashed line) for depth-averaged currents in 6-m depth due to variations in wind forcing. Currents were moderately sensitive to wind forcing.

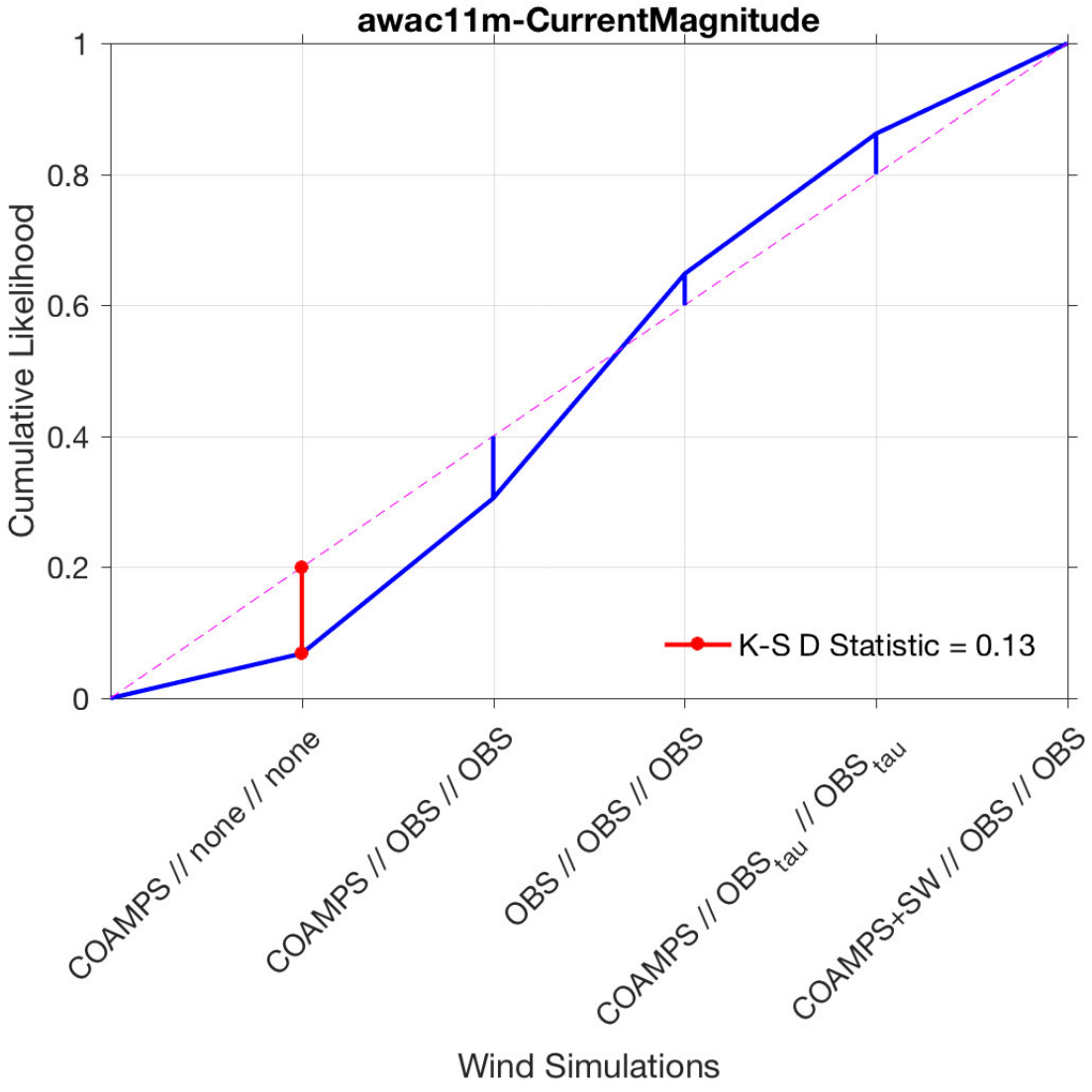

Figure 28.Cumulative likelihood distribution (blue line) and cumulative distribution where each parameter value is assigned equal probability (magenta dashed line) for depth-averaged currents due to variations in wind forcing. Currents were moderately sensitive to wind forcing based on K-S D statistic.

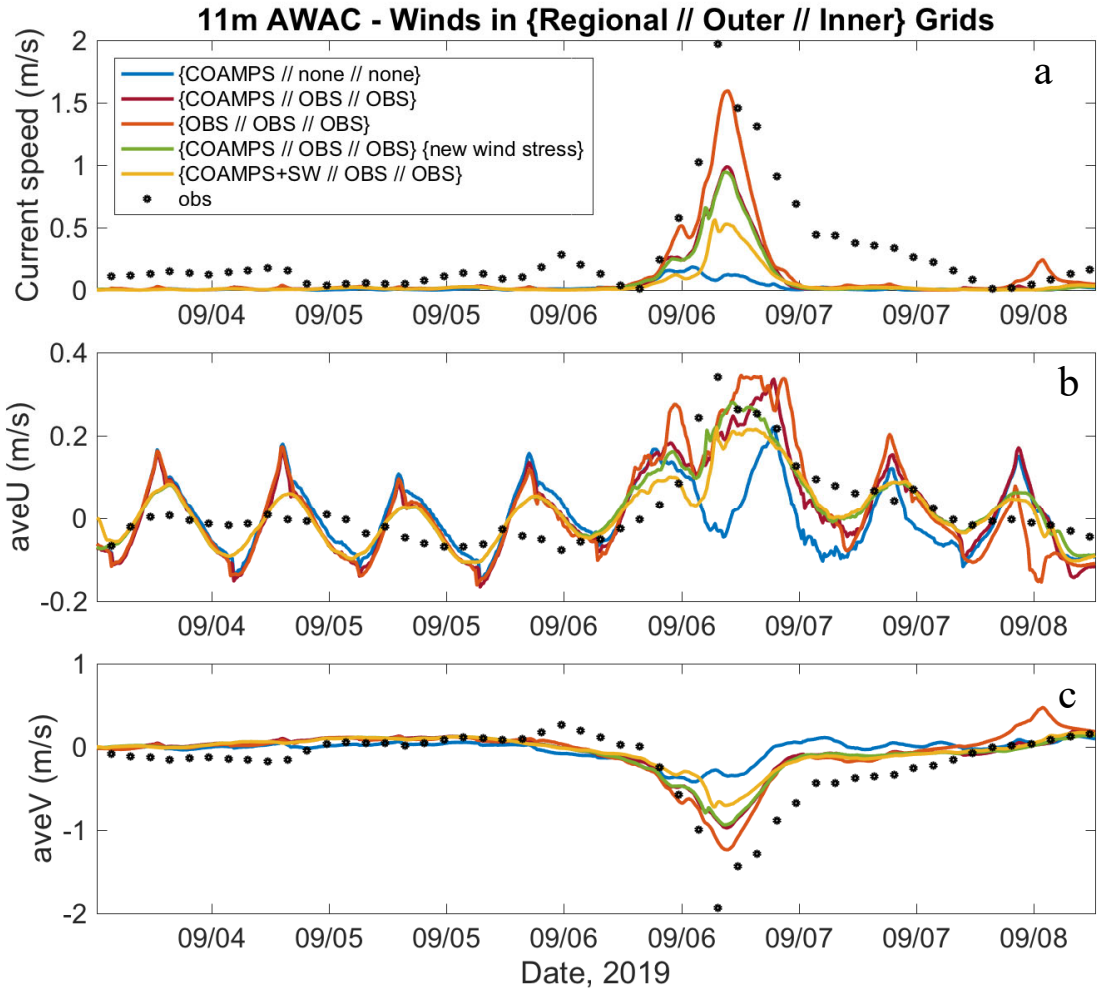

Figure 29. Timeseries of depth-averaged current a) magnitude, b) in the cross-shore direction, and c) in the along-shore direction at 11-m water depth under different wind forcing during Hurricane Dorian.

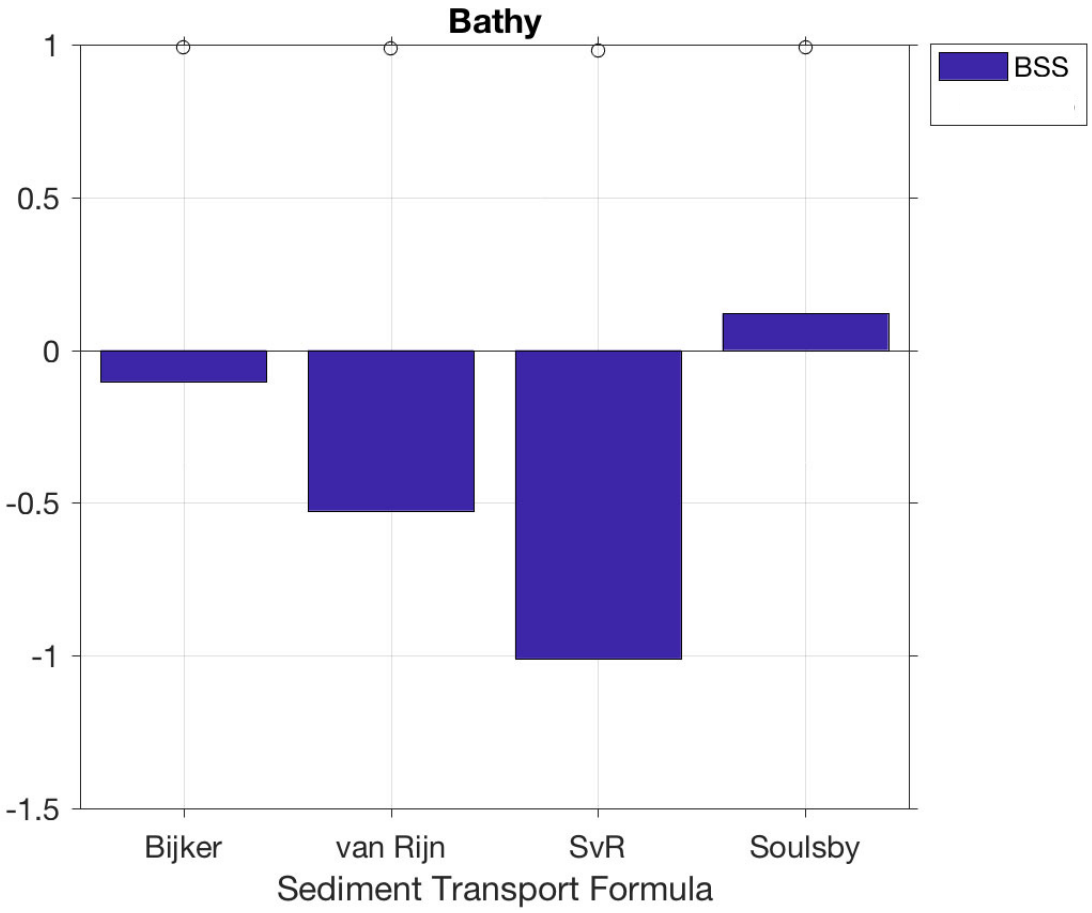

Figure 30. The Brier Skill Score (BSS) for simulated bathymetric change given different sediment transport formulations. Bathymetric change was moderately sensitive to the applied sediment transport formulation.

3.2. Delft3D-data comparison for 11 February Northeaster

A best model run was developed to confirm accurate model setup for the Jan – Feb munitions mobility experiment simulation period. We compared H_s, T_p, and wave direction at peak period, θ observed at the 17-m CDIP wave buoy and the 8-m wave and current profiler deployed in the same location as the munitions surrogates (Figure 9) with the WAVE simulation (Figure 31 and Figure 32). At the 17-m buoy, the model agreed very well with the observed H_s, with only slight differences in wave height during the peaks of the Northeaster storms. Modeled T_p also agreed well with observations throughout the simulation period with the largest differences occurring on 29 Jan and 3 Feb when T_p appeared to be shifting between sea (~5 sec) and swell (>10 s) bands. Modeled θ at the 17-m buoy varied during the passage of the storm, and the model tracked the observed change in θ well. Similarly, modeled H_s tracked observations well at the 8-m wave and current profiler, except during the peak of the storm on 11 Feb. Based on differences in observed wave height between the 17-m buoy and the 8-m wave and current

profiler, it appears that the wave height increased by nearly 2 m over a distance of ~3 km between the two instruments.

We compared depth-averaged current velocity observations at the 8-m wave and current profiler with the initial depth-averaged FLOW simulation (Figure 33). Simulated currents were underestimated for the passage of each Northeaster. Atmospheric conditions were forced with COAMPS for this simulation, so wind forcing was likely underestimated (see Figure 29 for sensitivity analysis of wind forcing), likely contributing to the underestimate of current speeds during storms.

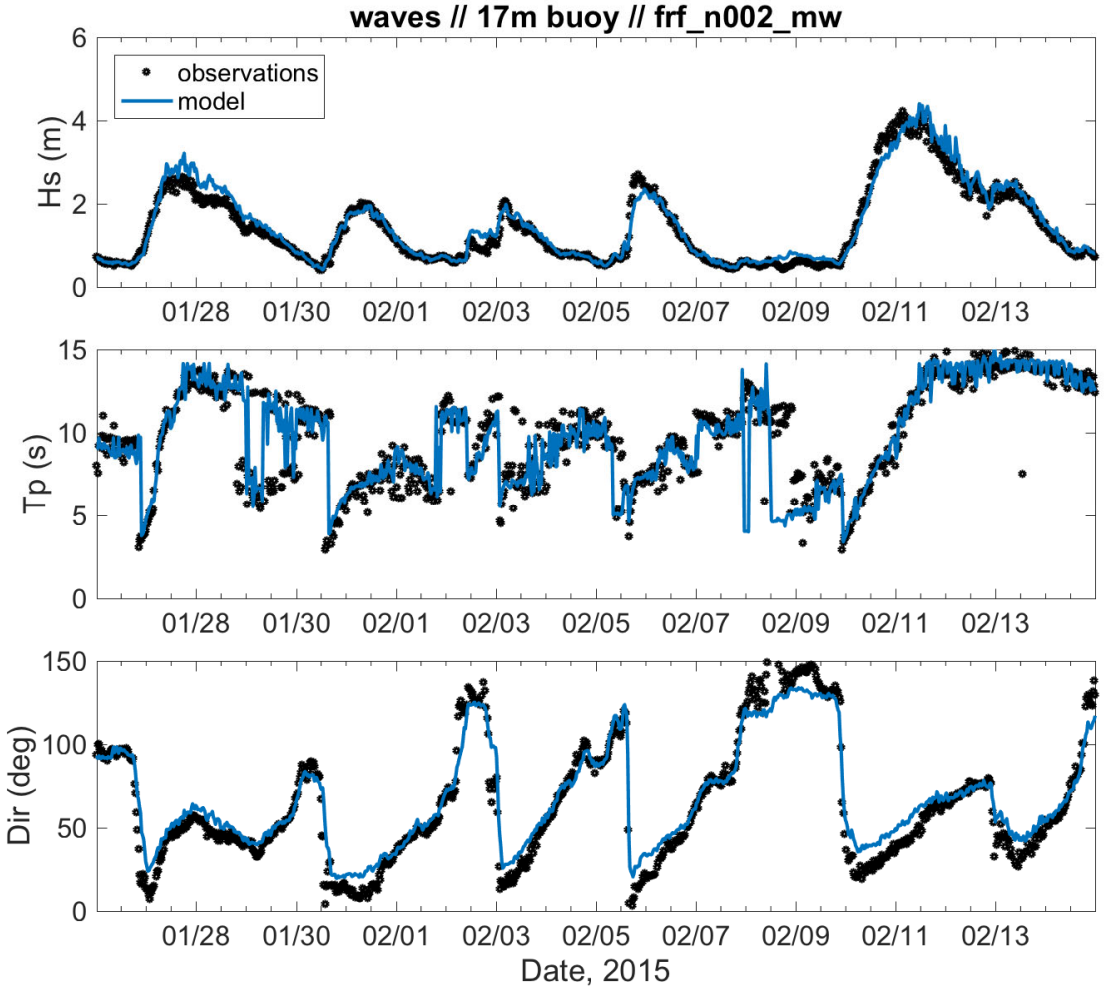

Figure 31. Comparison between modeled (blue line) and observed (black dots) time series of a) significant wave height, b) peak wave period, c) wave direction at peak period at the 17-m CDIP wave buoy. Location of the buoy is presented in Figure 9.

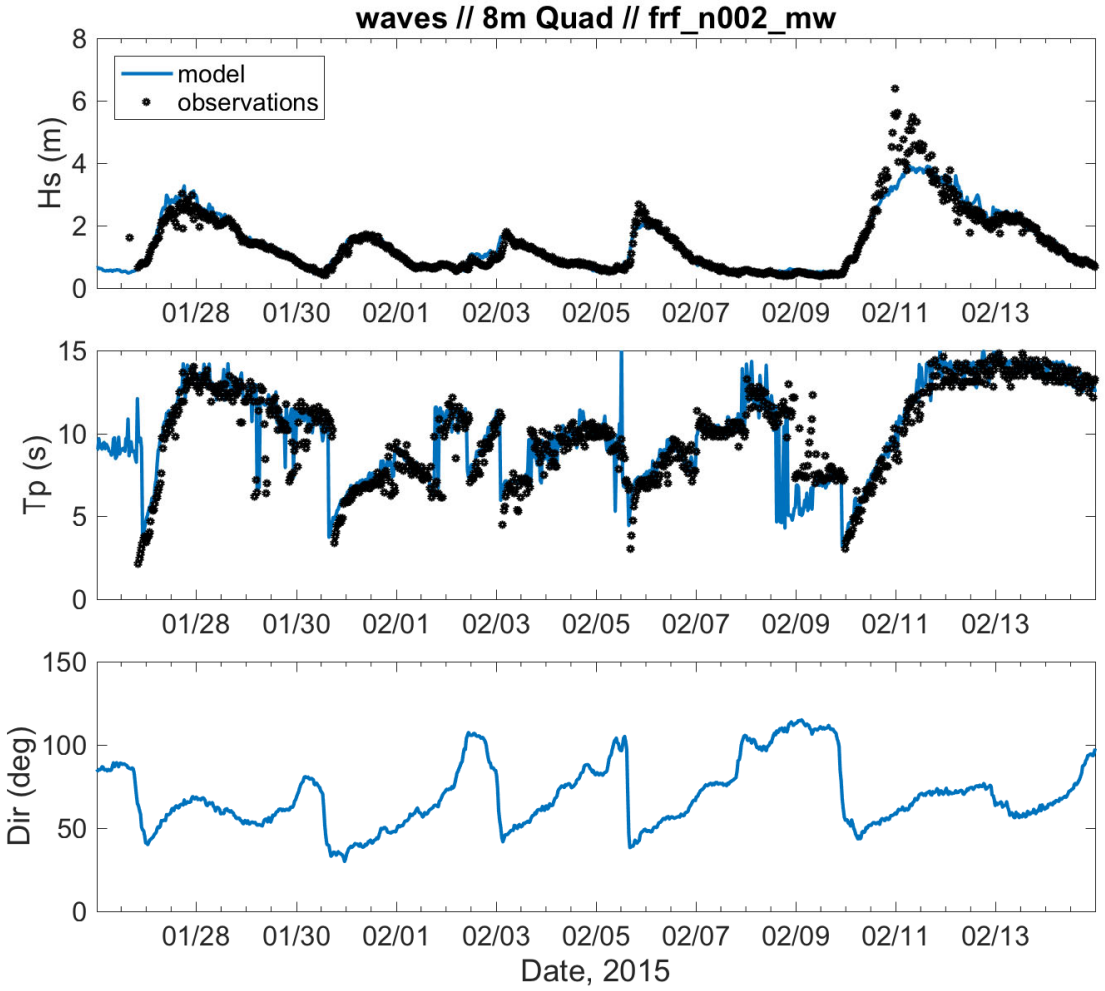

Figure 32. Comparison between modeled (blue line) and observed (black dots) time series of a) significant wave height, b) peak wave period, c) wave direction (observations not available) at peak period at the 8-m wave and current profiler. Location of the instrument is presented in Figure 9.

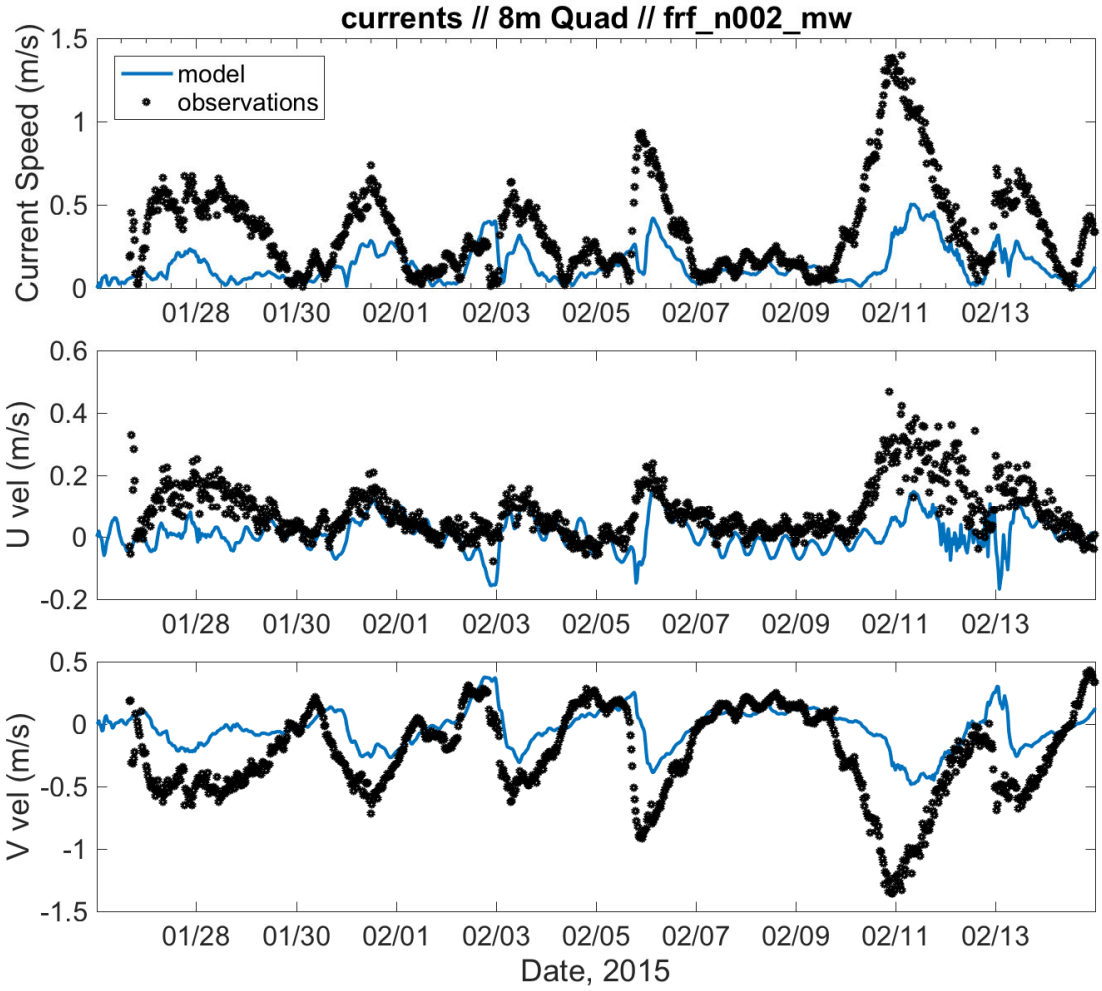

Figure 33. Comparison between modeled (blue line) and observed (black dots) a) current speed, b) cross-shore component of velocity, c) alongshore component of velocity at the 8-m wave and current profiler. Location of the 8-m wave and current profiler is presented in Figure 9.

3.3. Delft3D-UnMES results for 11 February Northeaster

Delft3D results were used to force UnMES during the peak of a Northeaster storm on 11 February 2015. Wave height at the offshore boundary of the inner model domain exceeded 4 m and decreased across the surf zone as wave energy dissipated due to wave breaking (Figure 34). Wave direction was nearly shore-perpendicular throughout the inner model domain (Figure 34). As expected from theory, wave period was nearly constant over the model domain at ~12 s, except where waves and currents interacted in the surf zone, resulting in wave periods above the range for which UnMES was trained (regions were wave period data is absent near the shoreline) (Figure 35). The depth-averaged current was primarily directed towards the south during the peak of the storm, except in the inner surf zone (Figure 36). Near-bed combined depth-averaged wave and current speed ranged between 0.9 and 1.2 m/s over most of the model domain

(Figure 37). The relative angle between wave direction and current direction was greater than 90º over most of the model domain (Figure 38).

Munitions mobility and burial were hindcast for a surrogate 81-mm mortar with specific gravity of 3. The probability of the surrogate munition remaining proud on the bottom was near 0 throughout the model domain (Figure 39). In contrast, probability of it fully burying was between 0.67 and 0.75 over most of the model domain (Figure 40). The probability of a migration distance between 0 and 5-m was between 0.94 and 0.99 over most of the model domain (Figure 41), while the probability of a migration distance between 5 and 50-m was near 0 (Figure 42). Although it is unlikely that the surrogate munition would migrate, the migration direction was estimated as more likely to be onshore than towards the south (compare Figure 43 and Figure 44).

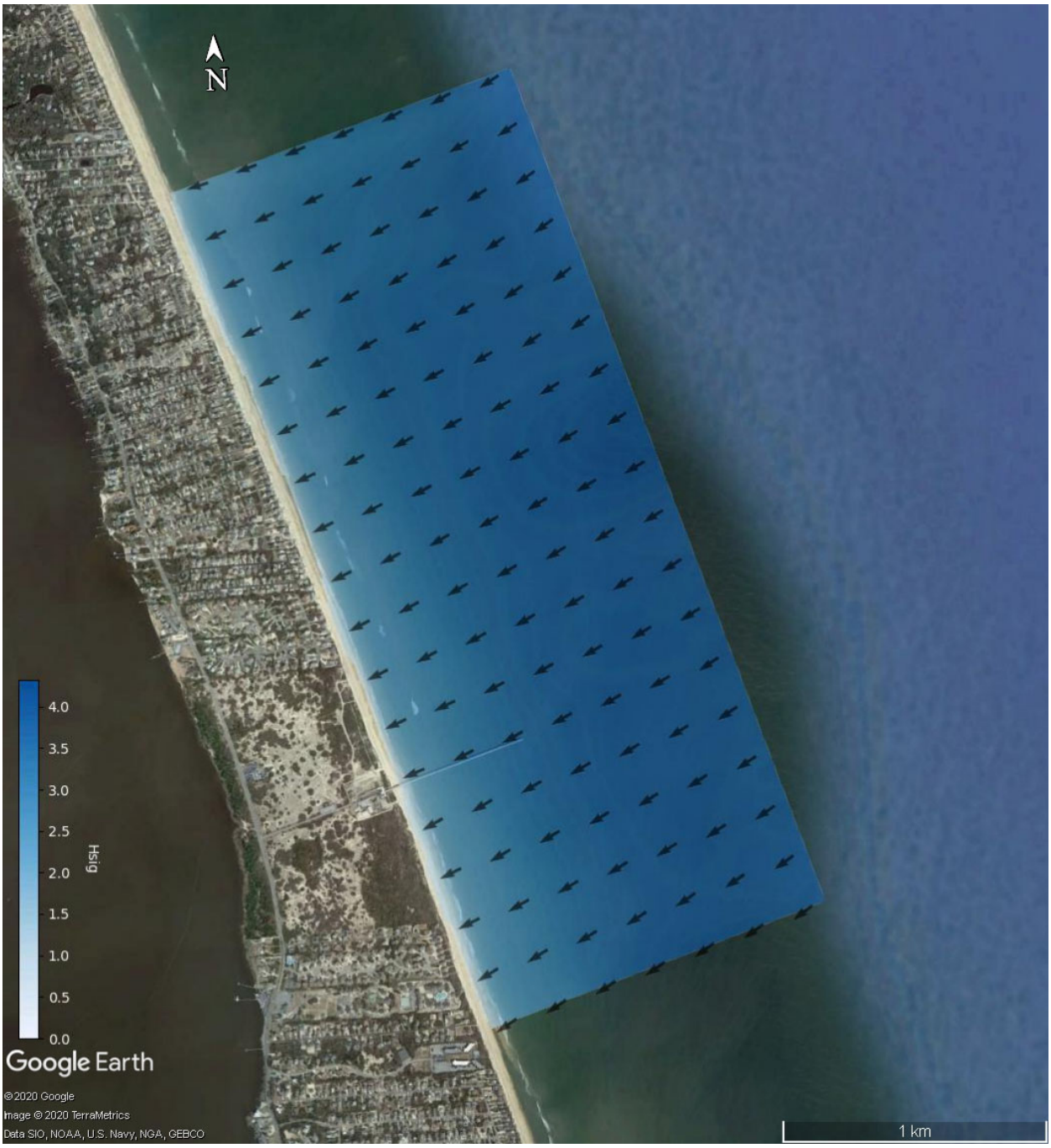

Figure 34. Modeled significant wave height and direction on 11 February 2015 0830 EST at the peak of the Northeaster storm used as input to UnMES.

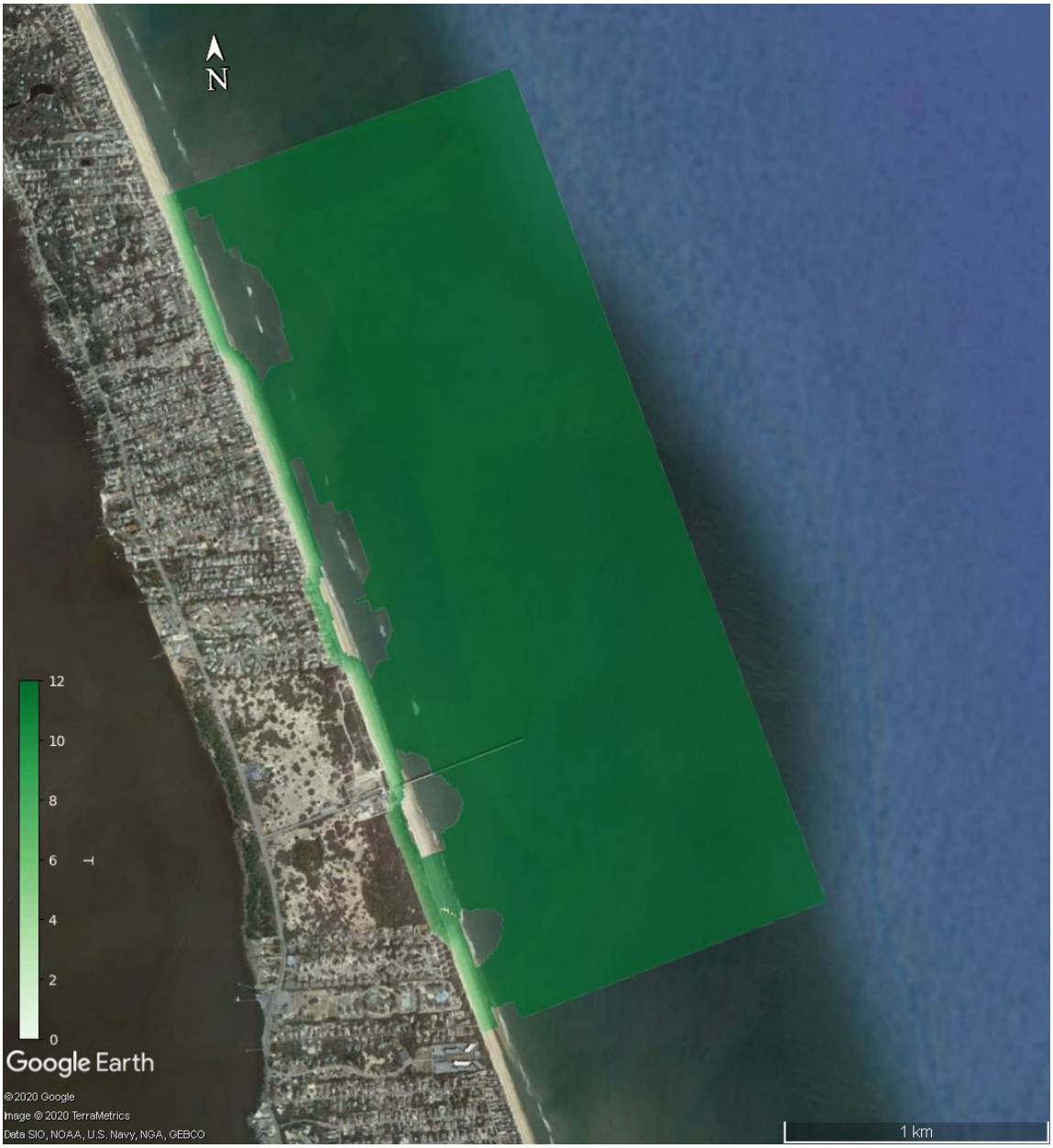

Figure 35. Peak wave period on 11 February 2015 0830 EST at the peak of the Northeaster storm used as input to UnMES. Regions near the shoreline where no model results are plotted indicate regions where the wave period exceeds the range with which the network was trained.

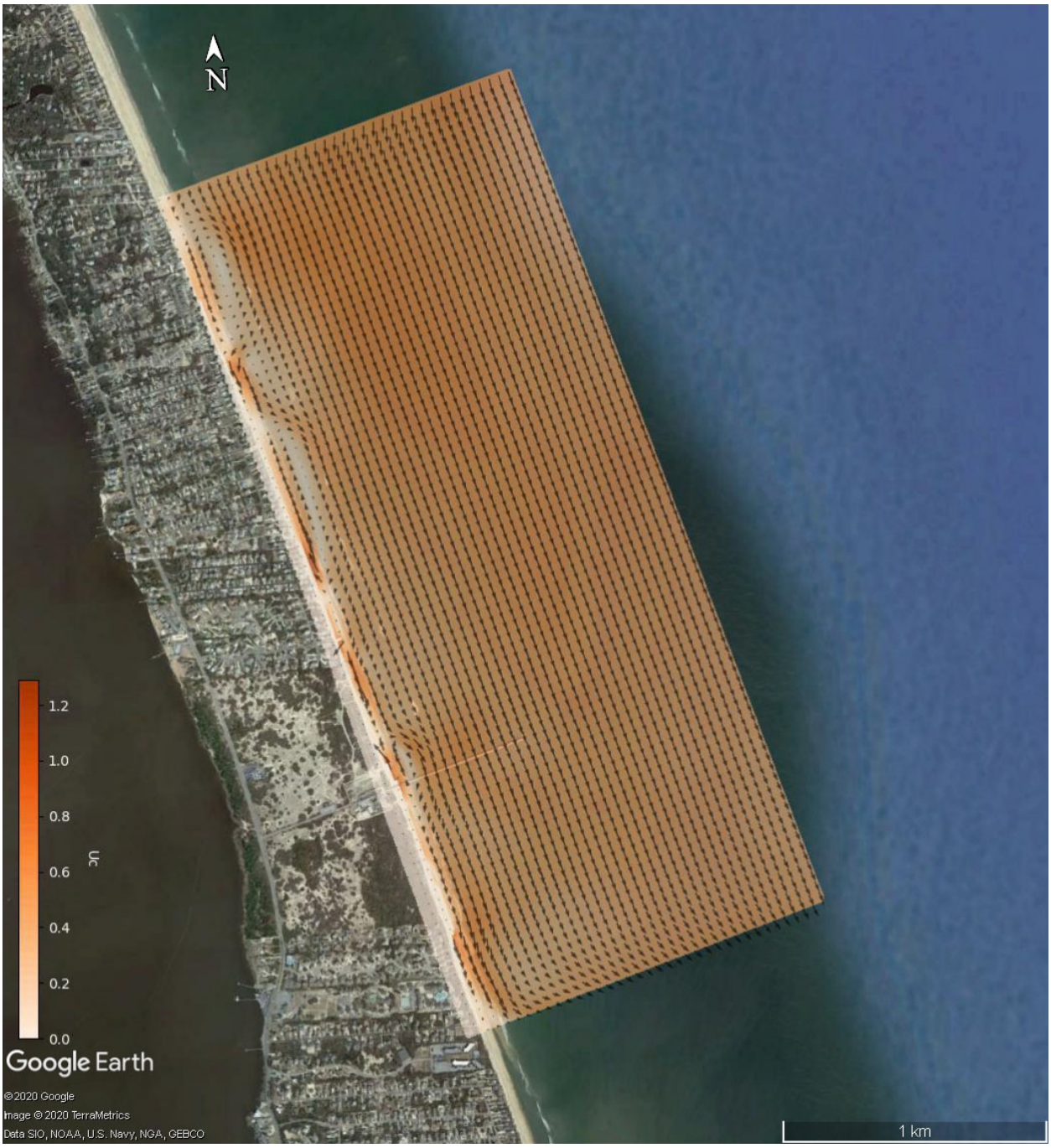

Figure 36. Depth-averaged current magnitude (color contours) and direction (black arrows) on 11 February 2015 0830 EST at the peak of the Northeaster storm.

Figure 37. Near-bed combined wave and current magnitude on 11 February 2015 0830 EST at the peak of the Northeaster storm used as input to UnMES. Regions near the shoreline where no model results are plotted indicate regions where the variable value exceeds the range with which the network was trained.

Figure 38. Angle between waves and currents on 11 February 2015 0830 EST at the peak of the Northeaster storm used as input to UnMES. Regions near the shoreline where no model results are plotted indicate regions where the variable value exceeds the range with which the network was trained.

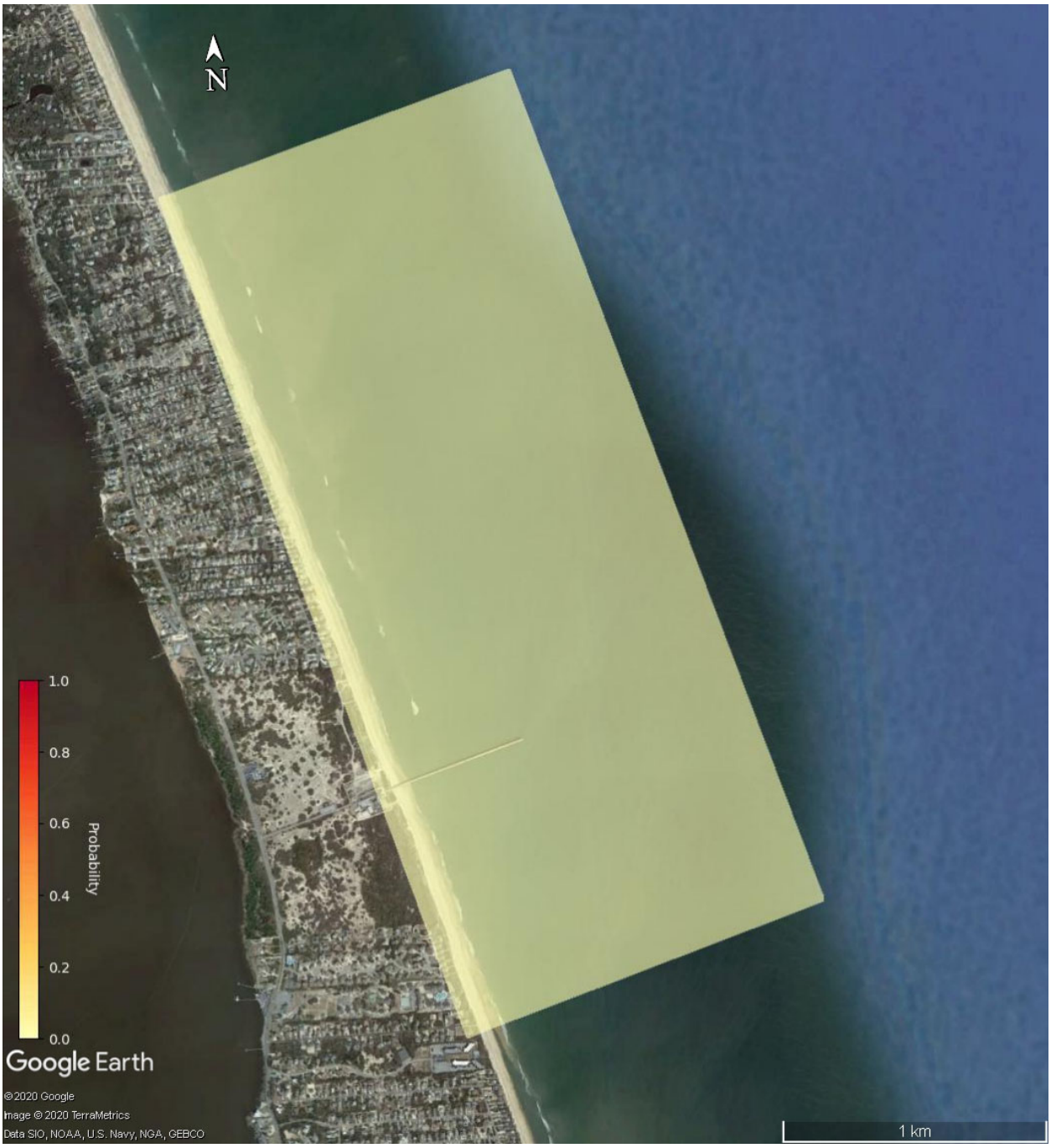

Figure 39. Estimated probability of surrogate 81-mm mortar remaining proud on the seafloor at the peak of the 11 February 2015 Northeaster.

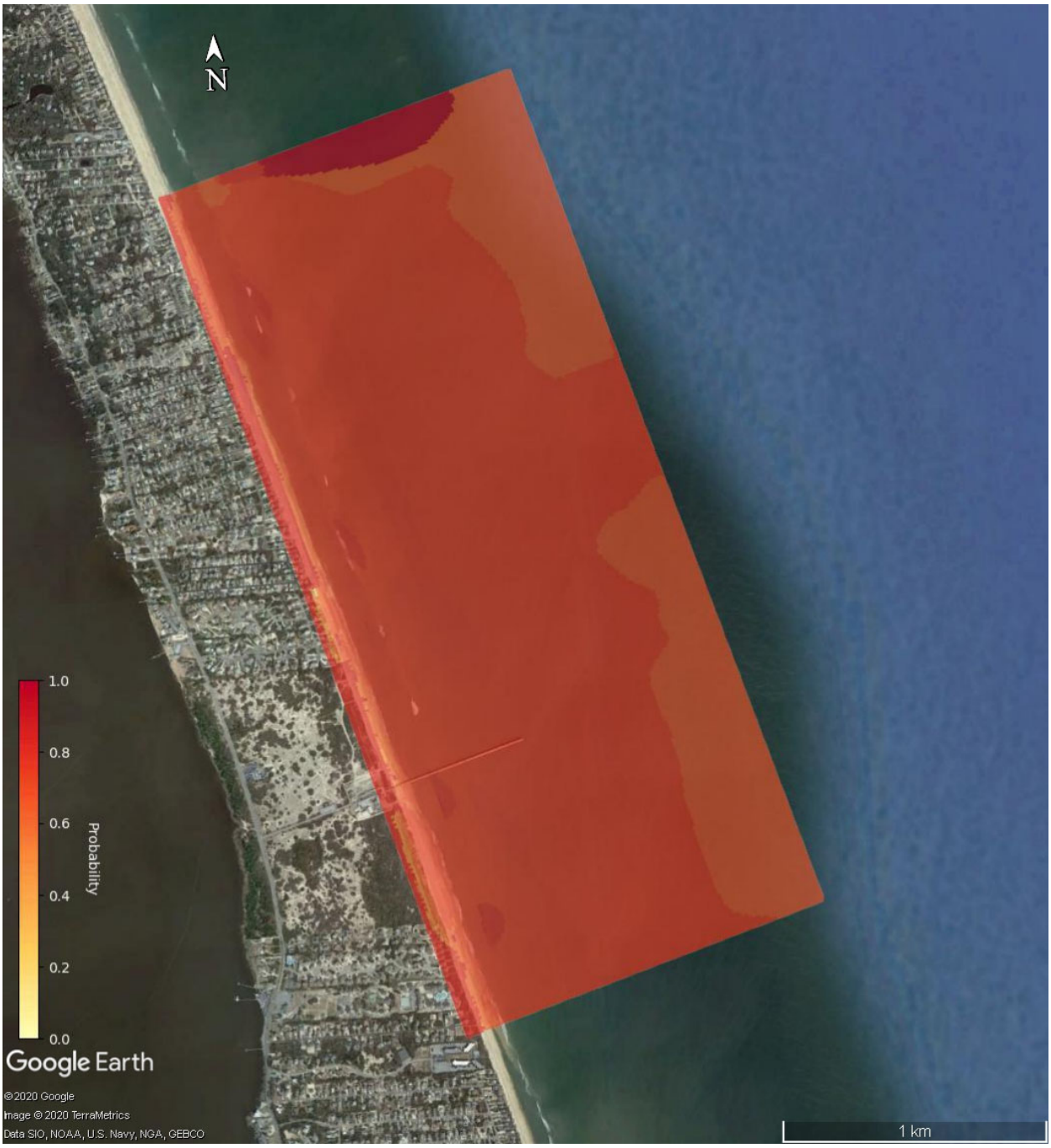

Figure 40. Estimated probability of surrogate 81-mm mortar fully burying into the seafloor at the peak of the 11 February 2015 Northeaster.

Figure 41. Estimated probability of surrogate 81-mm mortar migrating < 5 m during the peak of the 11 February 2015 Northeaster.

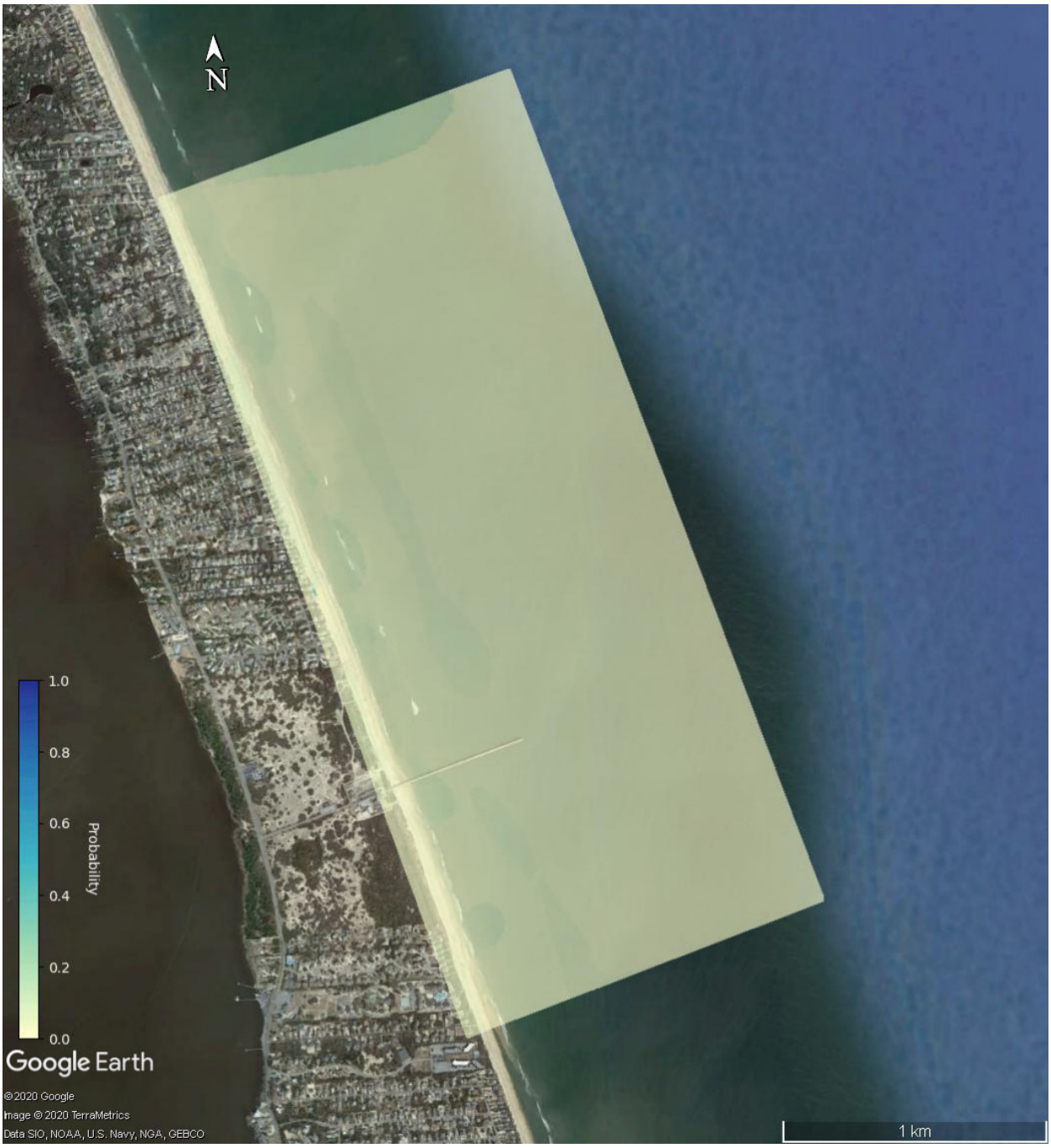

Figure 42. Estimated probability of surrogate 81-mm mortar migrating 5 to 50-m during the peak of the 11 February 2015 Northeaster.

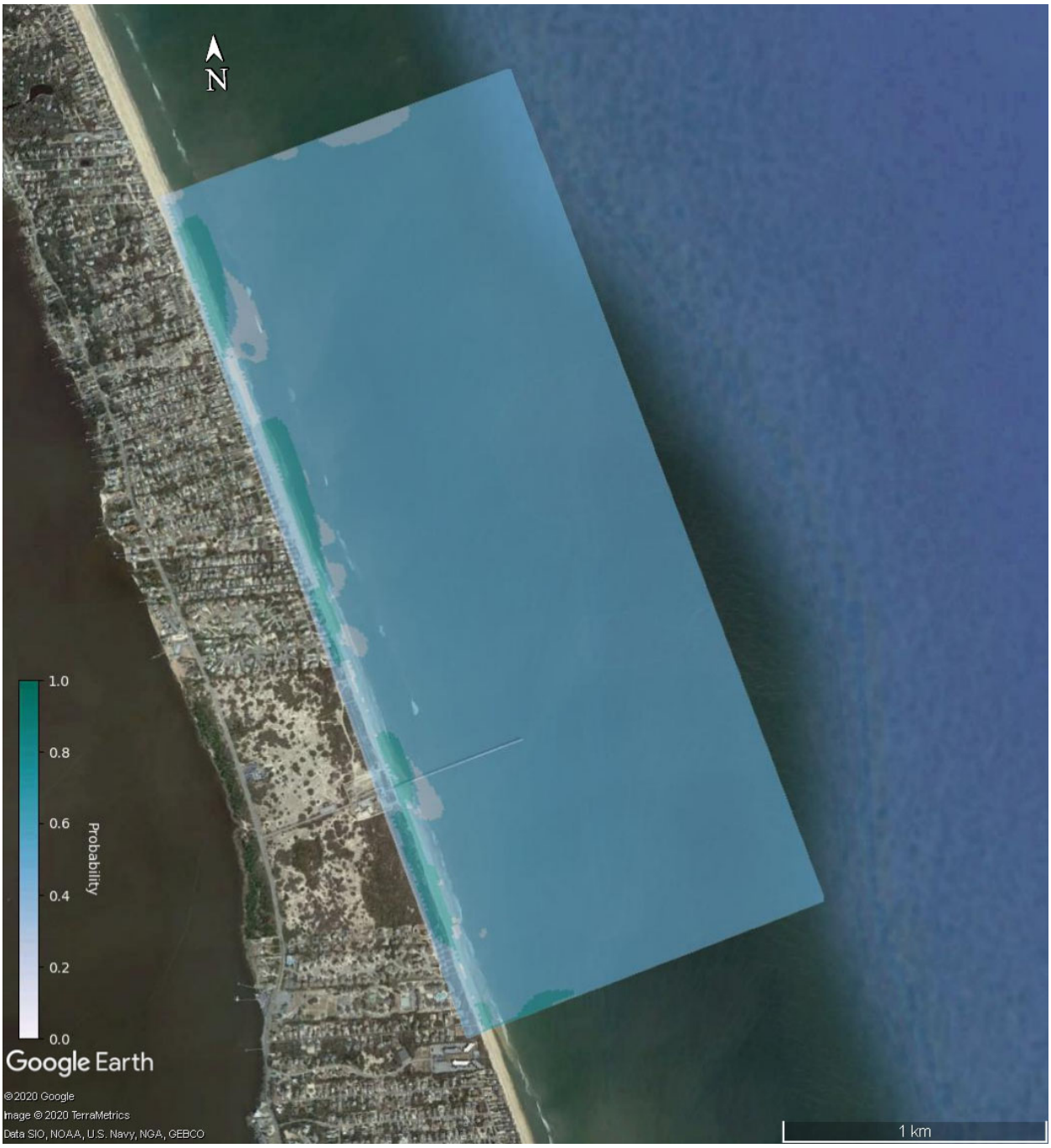

Figure 43. Estimated probability of surrogate 81-mm migrating onshore (+/-30^o relative to shore normal) during the peak of the 11 February 2015 Northeaster.

Figure 44. Estimated probability of surrogate 81-mm migrating towards the south (30º- 135º relative to shore normal) during the peak of the 11 February 2015 Northeaster.

3.4. Delft3D-UnMES comparisons to surrogate munitions observations 11 February Northeaster

The coupled Delft3D/UnMES model estimates of migration and burial of surrogate munitions compared favorably to observations. The model accurately represented the probability that a 81-mm mortar with specific gravity of 3 would bury during the peak of the 11 February Northeaster given information about

the munition type, the near bed velocity, the wave period, and the direction of waves and currents (Figure 45). Similarly, the model hindcast a high probability that the surrogate 81-mm mortar would remain in place during the storm (Figure 46).

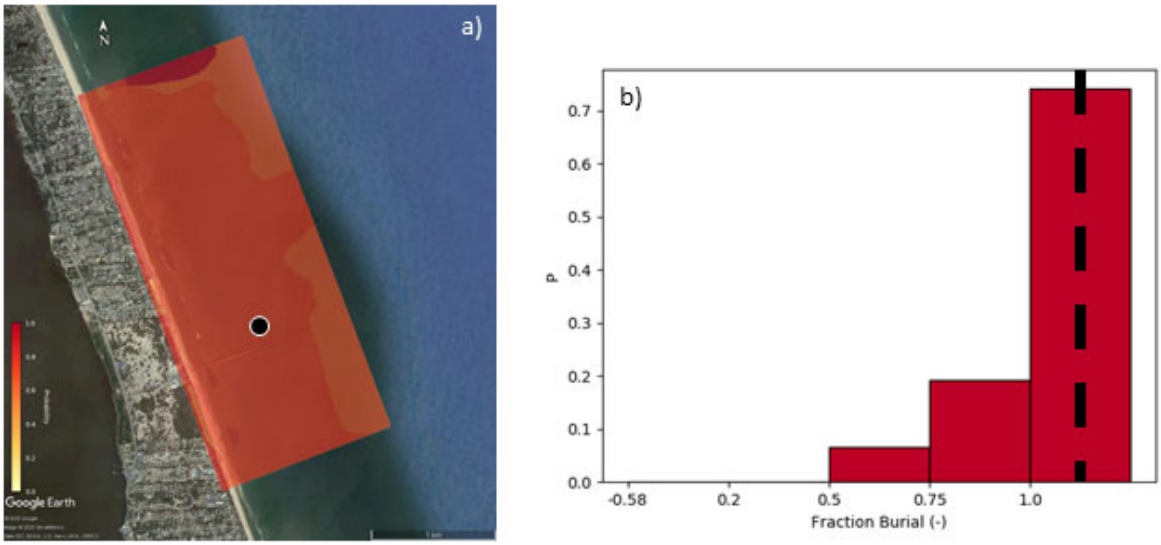

Figure 45. a) Estimated probability of total burial with surrogate 81-mm mortar (same as Figure 40). The location of surrogate munition observations is plotted as a black circle. b) The fraction of burial probability distribution. The full burial of the surrogate munition is represented as the dashed line.

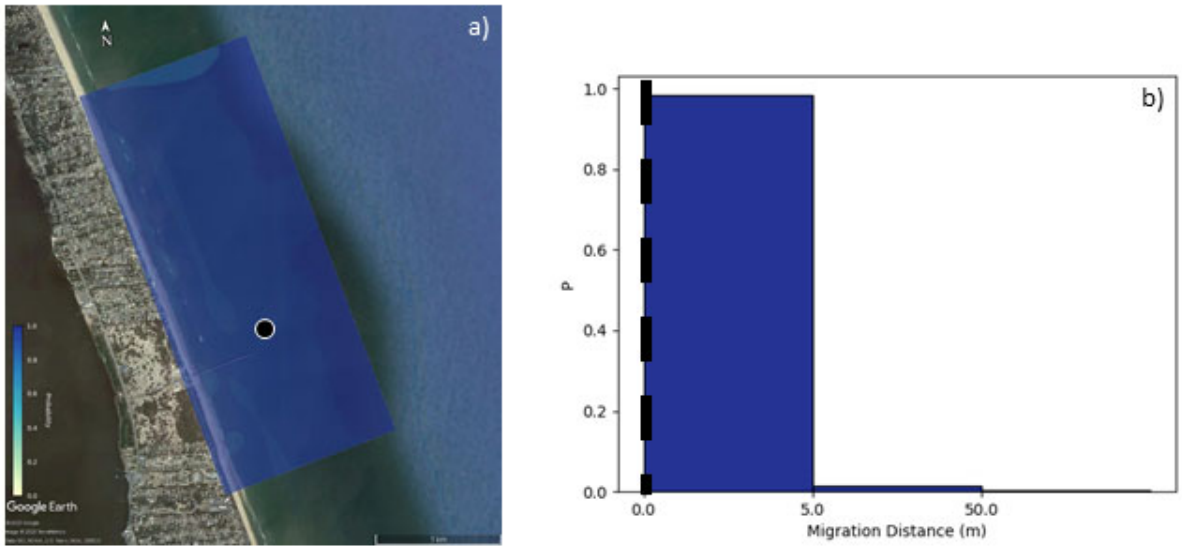

Figure 46. a) Estimated probability of migration distance of <5m for surrogate 81-mm mortar (same as Figure 41). The location of surrogate munition observation is plotted as black circle. b) The migration distance probability distribution. The migration distance of the surrogate munition is represented as the dashed line.

4. Discussion

4.1. Delft3D simulations

Our objective sensitivity analysis of depth-averaged currents in 6-m and 11-m depths using the GLUE method revealed a lack of sensitivity to the model coefficients and formulations that we varied. The implications of these findings are two-fold. First, it is not necessary to tune these coefficients to produce accurate estimates of depth-averaged currents. Second, coefficient variability contributes an insignificant amount to overall model error and uncertainty.

In contrast to model coefficients, depth-averaged currents were sensitive to wind forcing during high wind events. Analyses indicate that the underestimated COAMPS winds in coastal areas produce underestimated depth-averaged currents. In the Hurricane Dorian simulation, depth-averaged currents were underestimated by an order of magnitude using COAMPS winds. Although fetch is shorter in the outer and inner grids than in the regional US East grid, accurate wind speeds must be used to force the simulations in order to produce accurate depth-averaged currents. Using the observed wind speed and direction measured at the FRF pier to force the regional, outer, and inner grids produced results that compared best with the observed hydrodynamics. While local wind observations at the FRF pier are not accurate over the entire domain, forcing with observed winds produced the most accurate currents at our location of interest, so are preferable in absence of an accurate regional scale atmospheric model. Ongoing work is being conducted to identify improved regional-scale forcing and new wind stress coefficients are being tested to improve model stability.

Modeled bathymetric change was highly sensitive to the choice of sediment transport formulation. The most accurate sediment transport formulation was only moderately accurate, but did qualitatively reproduce observations of offshore sandbar migration (Figure 47). While the magnitude of the modeled change is less than observed, the modeled general patterns of erosion and accretion are very similar to the observations.

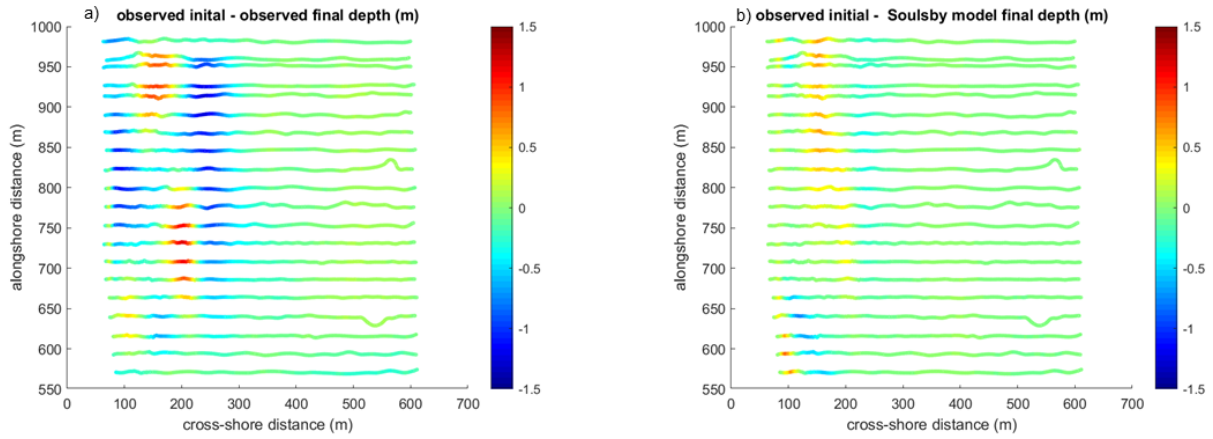

Figure 47. a) Comparison of change in surveyed bathymetry between 16 Sep 2015 and 8 Oct 2015 at the locations of raw survey data. b) Comparison of change in bathymetry between survey on 16 Sep 2015 and final simulated bathymetry on 8 Oct 2015 for simulation using the Soulsby sediment transport formulation. Simulated bathymetric changes in b) reproduced offshore bar migration observed in a).

4.2. Coupled Delft3D-UnMES simulations

The initial results testing the coupled Delft3D-UnMES model were promising. Modeled results from the peak of the 11 February 2015 Northeaster estimated high probabilities that munitions would bury in place, as was observed during the experiment. However, fully testing the probabilistic Delft3D/UnMES model will require significantly more observations of event occurrence/non-occurrence than a single storm can provide (e.g., Casati et al., 2008). We advocate following standard approaches and well established methods for assessing probabilistic model accuracy, which include (e.g., Casati et al., 2008; Holland et al., 2013):

- Calculation of threshold value statistics based on event occurrence/non-occurrence
    - Contingency table comparing true positives, false positives, true negatives, and false negatives (Morgan and Henrion, 1990)
    - Ambiguity table (Morgan and Henrion, 1990)
    - Relative operating characteristic (ROC) curve (Mason, 1982)
- Assessment of model reliability, sharpness (e.g., Jolliffe and Stephenson, 2003)
- Assessment of model sensitivity (e.g., Beuzen et al., 2018; Fienen and Plant, 2015)

The surrogate munitions field observations included in these analyses were limited to observations of burial, leaving the migration portion of the model largely untested. An additional complication of migration is that it may require a time integrated approach to accurately estimate migration distance. The coupled Delft3D-UnMES system may be modified to conduct the appropriate time integration.

5. Conclusions to date

Using our Delft3D model set up at Duck, NC, we conducted a sensitivity analysis of model coefficients, sediment transport formulae, and wind forcing using the Generalized Likelihood Uncertainty Estimate (GLUE). We found that model results were not sensitive to coefficients for Manning's friction coefficient,

horizontal eddy viscosity, or horizontal eddy diffusivity under the conditions that we tested. However, model results were sensitive to wind forcing and sediment transport formulae.

We developed a one-way coupled Delft3D-UnMES system. We then compared estimates of the probability of mobility and burial of an 81-mm mortar to observations of surrogate munitions behavior during a field experiment in Jan/Feb 2015 at the U.S. Army Corps of Engineers Field Research Facility (FRF) in Duck, NC. We found that our coupled model hindcasted a high probability of burial during the largest Northeaster storm during that period, consistent with observations. Based on our results from the munitions mobility hindcasts, we recommend additional testing of the coupled Delft3D-UnMES system using standard approaches for probabilistic model assessment; however, we recognize that obtaining many field observations of munitions mobility and burial will be difficult.

6. References

Aguilera, P.A., Fernández, A., Fernández, R., Rumí, R. and Salmerón, A., 2011. Bayesian networks in environmental modelling. Environmental Modelling & Software, 26(12): 1376-1388.

Beuzen, T. et al., 2018. Bayesian networks in coastal engineering: Distinguishing descriptive and predictive applications. Coastal Engineering, 135: 16-30.

Booij, N., Ris, R.C. and Holthuijsen, L.H., 1999. A third-generation wave model for coastal regions 1. Model description and validation. J. Geophys. Res., 104(C4): 7649-7666.

Casati, B. et al., 2008. Forecast verification: Current status and future directions. Meteorological Applications, 15(1): 3-18.

Charniak, E., 1991. Bayesian networks without tears. AI Magazine, 12(4): 50-63.

Fienen, M.N. and Plant, N.G., 2015. A cross-validation package driving netica with python. Environmental Modelling & Software, 63: 14-23.

Holland, K.T., Palmsten, M., Lalejini, D. and Spansel, S., 2013. Validation test report for probabilistic riverine bathymetry tool. In: D.o. Navy (Editor). Battlespace Awareness and Information Operations Program Office, Navy's Program Executive Office for C4I, San Diego, CA, pp. 1-98.

Jolliffe, I.T. and Stephenson, D.B., 2003. Forecast verification: A practitioners guide in atmospheric science. John Wiley and Sons, Chichester, England, 240 pp.

Lesser, G., Roelvink, J., Van Kester, J. and Stelling, G., 2004. Development and validation of a three-dimensional morphological model. Coastal engineering, 51(8): 883-915.

Mason, I., 1982. A model for assessment of weather forecasts. Aust. Meteor. Mag, 30(4): 291-303.

Morgan, M.G. and Henrion, M., 1990. Uncertainty: A guide to dealing with uncertainty in quantiative risk and policy analysis. Cambridge University Press, Cambridge, UK.

Norsys Software Corporation, 2011. Netica version 4.16.

Pearl, J., 1988. Probabilistic reasoning in intelligent systems: Networks of plausible inference. Morgan Kaufmann, San Francisco, CA, 552 pp.

Plant, N.G. and Holman, R.A., 1997. Intertidal beach profile estimation using video images. Marine Geology, 140(1–2): 1-24.

Rennie, S.E. and Brandt, A., 2015. Underwater munitions expert system to predict mobility and burial, Strategic Environmental Research and Development Program.

Simmons, J.A. et al., 2017. Calibrating and assessing uncertainty in coastal numerical models. Coastal Engineering, 125: 28-41.

Stauble, D.K., 1992. Long-term profile and sediment morphodynamics: Field research facility case history, COASTAL ENGINEERING RESEARCH CENTER VICKSBURG MS.

US Army Corps of Engineers, 2020. Chl thredds server.

Van Rijn, L.C., 1993. Principles of sediment transport in rivers, estuaries and coastal seas, 2. Aqua publications Amsterdam.

van Rijn, L.C. et al., 2003. The predictability of cross-shore bed evolution of sandy beaches at the time scale of storms and seasons using process-based profile models. Coastal Engineering, 47(3): 295-327.

Young, D.L., Bak, A.S. and Forte, M.F., 2018. Initialization and setup of the coastal model test bed: Integrated bathymetry, U.S. Army Engineer Research and Development Center, Vicksburg, MS.